https://doi.org/10.5194/egusphere-2025-1287
Preprint. Discussion started: 11 April 2025

Technical note: Sensitivity of the CAMS regional air quality modelling system to anthropogenic emission temporal variability

Marc Guevara[1], Augustin Colette[2], Antoine Guion[2], Valentin Petiot[3], Mario Adani[4], Joaquim Arteta[3], Anna Benedictow[5], Robert Bergström[6], Andrea Bolignano[4], Paula Camps[1], Ana C. Carvalho[6], Jesper Heile Christensen[7], Florian Couvidat[2], Ilia D'Elia[4], Hugo Denier van der Gon[8], Gaël Descombes[2], John Douros[9], Hilde Fagerli[5], Yalda Fatahi[10], Elmar Friese[11], Lise Frohn[7], Michael Gauss[5], Camilla Geels[7], Risto Hänninen[10], Kaj Hansen[7], Oriol Jorba[1], Jacek W. Kaminski[12], Rostislav Kouznetsov[10], Richard Kranenburg[8], Jeroen Kuenen[8], Victor Lannuque[2], Frédérik Meleux[2], Agnes Nyíri[5], Yuliia Palamarchuk[10], Carlos Pérez García-Pando[1,13], Lennard Robertson[6], Felicita Russo[4], Arjo Segers[8], Mikhail Sofiev[10], Joanna Struzewska[12], Renske Timmermans[8], Andreas Uppstu[10], Alvaro Valdebenito[5], Zhuyun Ye[7]

[1] Barcelona Supercomputing Center, Barcelona, 08034, Spain
[2] Institut National de l'Environnement Industriel et des Risques, Verneuil en Halatte, 60550, France
[3] Météo-France, Saint-Mandé, 94165, France
[4] ENEA: Italian National Agency for New Technologies, Energy and Sustainable Economic Development, Bologna, 40129, Italy
[5] MET Norway: Norwegian Meteorological Institute, Oslo, 0372, Norway
[6] SMHI: Swedish Meteorological and Hydrological Institute. Norrköping, SE-601 76, Sweden
[7] Aarhus University: Roskilde, 4000, Denmark
[8] TNO: Netherlands Organisation for applied scientific research, Utrecht, 3584, The Netherlands
[9] KNMI: Royal Netherlands Meteorological Institute, De Bilt, 3730, The Netherlands
[10] FMI, Finnish Meteorological Institute, Helsinki, 00-001, Finland
[11] Forschungszentrum Jülich GmbH, ICE-3, Institute of Climate and Energy Systems - Troposphere, 52428 Jülich, Germany
[12] IEP-NRI: Institute of Environmental Protection - National Research Institute, Warsaw, 00-001, Poland
[13] Catalan Institution for Research and Advanced Studies (ICREA), 08010, Barcelona, Spain

Correspondence to: Marc Guevara (marc.guevara@bsc.es)

Abstract. An accurate characterization of the temporal distribution in primary emissions is essential for air quality modeling. This study evaluates the impact of replacing the default temporal profiles in the Copernicus Atmosphere Monitoring Service (CAMS) European air quality multi-model ensemble with an updated dataset (CAMS-REG-TEMPO). The sensitivity of 11 regional models and the ensemble to these changes is assessed by comparing modeled and observed monthly, weekly, and diurnal cycles of nitrogen dioxide (NO_2), ozone (O_3), coarse particulate matter (PM_{10}), and fine particulate matter ($PM_{2.5}$) across Europe. NO_2 shows the greatest improvement, with weekly cycle correlations increasing up to +0.17 due to better road transport emissions representation. PM_{10} correlations improve in winter (up to +0.13 weekly and +0.07 diurnal) due to refined residential wood combustion emissions. $PM_{2.5}$ correlations remain largely unchanged, except for diurnal cycles, which improve in winter (+0.18) but slightly degrade in spring and summer (-0.02). O_3 is the least affected, as correlations were already high with default profiles (0.9–0.95). For some species and timescales (e.g., NO_2 diurnal cycles), results vary across models,

https://doi.org/10.5194/egusphere-2025-1287
Preprint. Discussion started: 11 April 2025

highlighting the complex interactions between emission timing and atmospheric processes. CAMS-REG-TEMPO has little effect on annual RMSE and bias, aside from slight improvements in high PM_{10} concentrations. Overall, the findings support implementing CAMS-REG-TEMPO in the operational CAMS multi-model ensemble.

1 Introduction

Air quality models require hourly emissions from primary pollutants to accurately represent dispersion and physico-chemical processes in the atmosphere. Numerous studies have demonstrated that a precise temporal distribution of emissions is crucial for capturing observed patterns from both ground-based and satellite observations (e.g., Mues et al., 2014; Fatahi et al., 2021, Skjøth et al. 2011, Baek et al., 2023; Grythe et al., 2019; Super et al., 2021). Despite the critical role of temporally resolved emissions on model performance, there are currently no international regulations mandating the reporting of emission inventories at such fine level of temporal disaggregation. As a result, emission inventories used for air quality modelling activities are typically provided at the annual or monthly levels. To achieve the necessary temporal granularity, emissions must be downscaled using predefined temporal weight factors at different levels: month-of-the-year (i.e., monthly), day-of-the-week (i.e., weekly) and hour-of-the-day (i.e., hourly) temporal weight factors.

At the European level, emission temporal profiles developed or derived from studies conducted in the late 1990s and early 2000's (e.g., Ebel et al., 1997) are still being widely used by multiple air quality modelling teams. This includes the European regional air quality production service provided by the Copernicus Atmosphere Monitoring Service (CAMS), which operationally delivers air quality daily analyses, forecasts and reanalyses through a multi-model ensemble approach (Colette et al., 2024). However, recent studies have identified limitations in these profiles, such as the reliance on outdated sources of information and failure to account for sociodemographic influences and climatological conditions (e.g., Backes et al., 2016; Athanasopoulou et al., 2017). Moreover, the recently revised Ambient Air Quality Directive 2024/2881/EC in Europe set more stringent standards to be attained by 2030, acknowledging modelling applications as a fundamental support in the assessment of air pollution. CAMS delivers operational products suited and designed for supporting the implementation of the AAQD, which pushes for continuous improvement of current products accuracy (e.g., de Meij et al., 2025). To overcome these challenges and improve the representation of temporal variations in emissions used for modelling applications, a new dataset of temporal profiles —CAMS-TEMPO— was recently developed within the CAMS framework (Guevara et al., 2021).

The aim of this study is to analyse and quantify the impact of implementing the new CAMS-TEMPO anthropogenic temporal profiles on the performance of the CAMS multi-model ensemble. The sensitivity of the 11 regional models that comprise the CAMS ensemble is assessed by comparing modelling results against observations from a European network of air quality ground-based stations. The analysis how changes in emission temporal distribution affect the ability to reproduce observed monthly, weekly and diurnal cycles of four key air pollutants: nitrogen dioxide (NO_2), ozone (O_3), particulate matter (PM_{10})

https://doi.org/10.5194/egusphere-2025-1287
Preprint. Discussion started: 11 April 2025

and fine particulate matter ($PM_{2.5}$). Changes in the average deviation from observations are also analysed. A key contribution of this study, compared to previous research on emission temporal variations (e.g., Mues et al., 2014), is its comprehensive evaluation across multiple models. By drawing conclusions from a diverse ensemble rather than individual models, this approach minimizes the risk of error compensation and provides a more robust assessment of emission temporal effects on air quality modelling. Testing the impact of changing emission temporal profile with a single model carries a risk to correct a bias which would be actually due to the misrepresentation of other factors affecting the daily or seasonal variability (typically planetary boundary layer or insolation variability). While we cannot rule out that such misrepresentation occur in several models, it is relatively unlikely that it would act in the same direction in the whole ensemble. That is why the ensemble approach mobilised here argues in favour of the robustness of the diagnostic

The methods and data used in this work are presented in Sect. 2. The results section (Sect. 3) discusses the temporal distribution analysis for primary emissions, and the temporal correlation analysis and the mean deviation analysis for modelled air pollutant concentrations. Finally, Sect. 4 summarises the main conclusions and lessons learned.

2 Method and data

2.1 The CAMS regional air quality modelling system

The CAMS regional service (https://atmosphere.copernicus.eu/european-air-quality-forecast-plots/) provides daily 4-day forecasts for key air quality species along with analyses of the previous day, and retrospective reanalyses using the latest observation datasets available for assimilation. As the reference air quality forecasting system at the European scale, it operates through a distributed network of eleven Chemical Transport Models (CTMs) across ten European countries (described in Table 1), coordinated by a Centralised Regional Production Unit to ensure consistency. Using an ensemble of CTMs enhances forecast reliability by reducing the risk of failure in daily production and improving the skill of the forecast (Galmarini et al., 2013). Detailed information on the CAMS regional air quality production system and the individual models within the ensemble can be found in Colette et al. (2024). While each model differs in its design with regards to internal physical and chemical processes, strong common requirements exist in the CAMS regional service with regards to forcing meteorological data, chemical boundary conditions at the European boundary, and anthropogenic emissions.

Table 1 Chemistry transport models participating in the CAMS regional ensemble system

Model name	Institute (country)	Reference
CHIMERE	INERIS (France)	Menut et al. (2021)
DEHM	AARHUS UNIVERSITY (Denmark)	Christensen (1997), Brandt et al. (2012), Geels et al. (2021), Frohn et al. (2002 and 2021)
EMEP	MET Norway (Norway)	Simpson et al. (2012), EMEP MSC-W (2022)

https://doi.org/10.5194/egusphere-2025-1287
Preprint. Discussion started: 11 April 2025

EURAD-IM	FZJ ICE-3 (Germany)	Franke et al. (2024), Friese and Ebel (2010)
GEM-AQ	IEP-NRI (Poland)	Kaminski et al. (2008), Struzewska and Kaminski (2008)
LOTOS-EUROS	KNMI, TNO (The Netherlands)	Manders et al. (2017)
MATCH	SMHI (Sweden)	Roberston et al. (1999); Andersson et al. (2007)
MINNI	ENEA (Italy)	D'Elia et al. (2021); Mircea et al. (2014)
MOCAGE	Meteo-France (France)	Josse et al. (2004), Sič et al. (2015); Guth et al. (2016)
MONARCH	BSC (Spain)	Badia et al. (2017), Klose et al. (2021), Navarro-Barboza et al. (2024), Pérez et al. (2011)
SILAM	FMI (Finland)	Sofiev et al. (2015, 2010 and 2018), Sofiev (2002), Kouznetsov and Sofiev (2012)

2.2 Emission inputs

The CAMS European regional air pollutant emission inventory (CAMS-REG-AP_v4.2; Kuenen et al., 2022) is used to represent anthropogenic emissions. This inventory uses official annual air pollutant emissions submitted by each country to the European Monitoring and Evaluation Programme (EMEP) and performs a spatial mapping to a grid of 0.1x0.05 degrees using appropriate surrogate statistics for each activity. Biomass burning emissions are derived from the CAMS Global Fire Assimilation System (GFAS; Kaiser et al., 2012) across all CAMS regional models, while emissions from other natural sources such as biogenic, sea salt and desert dust are estimated by each model system using dedicated and diverse on-line parametrisations, as detailed in the references summarised in Table 1.

2.3 Anthropogenic temporal profiles

2.3.1 Default profiles

Table 2 summarises the default temporal profiles used by each model in the CAMS regional production service at the time of performing this study. Most of the models (7 out of 11) perform the temporal disaggregation of the anthropogenic emissions using the profiles constructed by the Netherlands Organisation for Applied Scientific Research (TNO; Denier van der Gon et al., 2011), while the remaining models use the temporal factors from the Generation of European Emission Data for Episodes project (GENEMIS) (Ebel et al., 1997; Friedrich and Reis, 2004). Both datasets were developed at European level and include monthly, weekly and diurnal temporal profiles.

GENEMIS monthly and weekly profiles vary per sector and country, while hourly profiles vary per sector only. The profiles were determined using various indicators, including fuel use, power plant load curves, temperature, degree days, working hours, traffic counts and fertilizer use, among others (Lenhart and Friedrich, 1996). In contrast, TNO profiles are sector-dependent only across all timescales (monthly, weekly and hourly) and largely based on GENEMIS data and older Western European datasets. For example, road transport profiles are based on Dutch traffic count data from 1985-1998, while energy sector profiles are derived from Veldt (1992). Livestock emissions in TNO profiles are based on Skjøth et al. (2011). The

https://doi.org/10.5194/egusphere-2025-1287
Preprint. Discussion started: 11 April 2025

hourly sector-dependent profiles in GENEMIS and TNO are identical. In the CHIMERE and EMEP models, the GENEMIS hourly weight factors for road transport are replaced by country- and day-of-the-week-dependent profiles developed by Menut et al. (2012), which were derived from measured surface NO_2 concentrations at European traffic stations.

Table 2 Summary of the default emission temporal profiles used by the CAMS regional models

Dataset	Monthly profiles	Weekly profiles	Hourly profiles	Models
TNO profiles	Sector-dependent	Sector-dependent	Sector-dependent[(1)]	EURAD-IM, GEM-AQ, LOTOS-EUROS, MINNI, MOCAGE, MONARCH, SILAM
GENEMIS profiles	Sector- and country-dependent	Sector- and country-dependent		CHIMERE[(2)], DEHM, MATCH, EMEP[(2)]

[(1)] The hourly sector-dependent profiles in GENEMIS and TNO are identical
[(2)] Hourly factors for road transport from Menut et al. (2012), which are country- and day-of-the-week-dependent

2.3.2 CAMS-REG-TEMPO profiles

The CAMS REGional TEMPOral (CAMS-REG-TEMPO) dataset consists of a collection of European regional temporal factors aligned with the domain specifications (resolution and geographical coverage) and sector classification of the CAMS-REG-AP emission inventory. It includes monthly, weekly, daily (day-of-the-year) and hourly temporal profiles for the key air pollutants (NO_x, SO_2, NMVOCs, NH_3, CO, PM10, PM2.5). Temporal profiles vary in spatial representation depending on the pollutant source and temporal resolution (i.e., monthly, weekly, daily, hourly): some are spatially invariant (i.e., a unique set of temporal weights for the entire domain), while others are spatially variant (i.e., temporal weights vary by grid cell or country). Additionally, profiles may be year-dependent and/or pollutant-dependent, depending on the characteristics of the input data and the approaches to compute the profiles. The dataset is built using a wide range of data sources Multiple sources of information –including energy statistics and measured activity data, among others–and meteorology-dependent parametrizations such as the heating degree day approach. A detailed description of the datasets and parametrizations is available in Guevara et al. (2021).

This study considers an updated version of the CAMS-REG-TEMPO dataset first presented in Guevara et al. (2021). The key updates in this new version (v3.2) compared to the previous release (v2.1) are as follows:

- Road transport (GNFR_F): Updated monthly temporal profiles for urban and rural areas were developed to distinguish between urban and interurban road traffic activities. Urban profiles were derived from TomTom congestion statistics for European cities (https://www.tomtom.com/en_gb/traffic-index/). These city level profiles were aggregated to the country level based on the annual average congestion and city population. Rural profiles were constructed using a

https://doi.org/10.5194/egusphere-2025-1287
Preprint. Discussion started: 11 April 2025

wide range of traffic count datasets from national road administrations (Table S1). The classification of urban and rural areas within the CAMS-REG-AP grid follows the Global Human Settlement Layer (GHSL) dataset (Pesaresi et al., 2019). New weekly and hourly temporal profiles were also constructed using TomTom congestion statistics, but without differentiating between urban and rural areas.

- Aviation (GNFR_H): In v2.1, a flat (i.e., no variation across time steps) weekly profile was assumed for this sector. In v3.2, country-dependent weekly profiles were introduced, derived from daily air traffic statistics at national airports from 2016 to 2019 provided by EUROCONTROL (2020). These profiles were aggregated at the country level based on the available national airport data.
- Shipping (GNFR_G): Previously, no monthly variations were considered for this sector. In v3.2, sea region- and pollutant-dependent monthly profiles were developed using CAMS-GLOB-SHIP_v2.1 AIS-based monthly emissions (Jalkanen et al., 2016). The new profiles vary per pollutant and sea region but are considered yearly independent due to minimal year-to-year variations.
- Other mobile sources (GNFR_I): In v2.1, flat monthly, weekly and hourly profiles were assumed for this sector. In v3.2, pollutant-dependent monthly, weekly and hourly profiles were developed using the profiles reported in the EMEP/EEA emission inventory guidebook (EMEP/EEA, 2019) and the MapEIre project (https://projects.au.dk/mapeire/). The profiles reported by EMEP/EEA (2019) include temporal weight factors for Agriculture and Forestry, Industry and Construction, Household and Gardening and Military subcategories. The weight factors for the Commercial and Institutional subcategory were derived from MapEire as they are not included in EMEP/EEA (2019). Subcategory profiles were averaged at the GNFR_I level based on their contributions to total GNFR_I emissions, estimated considering the 2018 EMEP official reported emission data for the EU27 plus UK (EMEP/CEIP, 2021).
- Data gap-filling procedure: In version 2.1, TNO profiles were applied by default in countries where local proxies (e.g., electricity production, air traffic statistics) were unavailable. In the v 3.2, a more refined approach was adopted by constructing averaged profiles from countries within the same world region, based on world region definitions from the EDGAR emission inventory (Crippa et al., 2018).

Table 3 summarizes the characteristics of each profile included in the CAMS-REG-TEMPO dataset for each sector and temporal resolution. For the fugitive fossil fuel (GNFR_D), use of solvents (GNFR_E) and waste management (GNFR_J) sectors, as the profiles remain unchanged from those reported by TNO due to lack of more detailed information. However, it is important to highlight that these sectors contribute minimally to total primary European emissions for all pollutants. An exception is GNFR_E (solvent use), which accounts for approximately 35% of total NMVOC at the EU27 level (EMEP/CEIP, 2021).

https://doi.org/10.5194/egusphere-2025-1287
Preprint. Discussion started: 11 April 2025

To facilitate the integration of the CAMS-REG-TEMPO profiles into CAMS regional models, the gridded profiles were simplified to a country-level format. This process involved combining the original CAMS-REG-TEMPO gridded profiles with the CAMS-REG-AP_v4.2 annual inventory to generate gridded monthly and daily emissions using the HERMESv3_GR emission processing system (Guevara et al., 2019). The resulting monthly and daily gridded emissions were then averaged at the country level and normalized to produce country- and pollutant-dependent simplified profiles. This simplification was applied to all emission temporal profiles provided at the grid cell level (Table 3), including monthly profiles for the GNFR_F sector (all species) and daily temporal profiles for the GNFR_C sector (all species), GNFR_K (livestock emissions, NH_3 and NO_x) and GNFR_L (other agricultural emissions, NH_3).

Table 3 Main characteristics of the CAMS-REG-TEMPO_v3.2 dataset. Per country: indicates that the profiles vary per country; per pollutant: indicates that the profiles vary per pollutant; per grid cell: indicates that the profiles vary per grid cell within a country; per year: indicates that the profiles vary per year; fixed: indicates that the profiles are spatially invariant. The symbol "-" denotes that no profile is proposed.

Sector	Description	Monthly	Daily	Weekly	Hourly
GNFR_A	Public Power	per country, pollutant	-	per country, pollutant	per country, pollutant
GNFR_B	Industry	per country	-	fixed (1)	fixed (1)
GNFR_C	Other stationary combustion		per grid cell, year		per pollutant
GNFR_D	Fugitive fossil fuel	fixed (1)	-	fixed (1)	fixed (1)
GNFR_E	Solvents	fixed (1)	-	fixed (1)	fixed (1)
GNFR_F1	Road transport exhaust gasoline	per year, grid cell for CO and NMVOC; per grid cell for others	-	per country	per country, day type(2)
GNFR_2	Road transport exhaust diesel	per year, grid cell for NO_x; per grid cell for others	-	per country	per country, day type
GNFR_F3	Road transport exhaust LPG	per grid cell	-	per country	per country, day type
GNFR_F4	Road transport non-exhaust (wear and evaporative)	per grid cell for PM; fixed for NMVOC	-	per country for PM; fixed for NMVOC	per country, day type for PM; fixed for NMVOC
GNFR_G	Shipping	per sea region and pollutant	-	fixed (1)	fixed (1)
GNFR_H	Aviation	per country	-	per country	fixed
GNFR_I	Off road transport	fixed, per pollutant	-	fixed, per pollutant	fixed, per pollutant
GNFR_J	Waste management	fixed (1)	-	fixed (1)	fixed (1)
GNFR_K	Agriculture (livestock)	fixed for others than NH_3 and NO_x	per grid cell, year for NH_3 and NO_x	fixed for others than NH_3 and NO_x(1)	fixed(1)

https://doi.org/10.5194/egusphere-2025-1287
Preprint. Discussion started: 11 April 2025

GNFR_L	Agriculture (fertilizers, agricultural waste burning)	per country for others than NH_3	per grid cell, year for NH_3	(fixed for others than NH_3)[(2)]	fixed, per pollutant

[(1)] Same profile as the one reported by the TNO dataset (Denier van der Gon et al., 2011)
[(2)] Day types are weekday (Monday to Friday), Saturday and Sunday

2.4 Observational dataset and evaluation statistics

The observational dataset considered for the model evaluation was acquired from the European Environment Agency (EEA) through the download service https://discomap.eea.europa.eu/map/fme/AirQualityExport.htm (last accessed, May 2023). Collected data corresponds to the E1a validated dataset where we keep only data with an hourly timestep. The E1a data are reported to EEA by member states every September, covers the year before the delivery and are considered an official delivery. Pollutants included in the evaluation are O_3, NO_2, PM_{10} and $PM_{2.5}$. Then, only measurements that are considered representative of scale that the models are able to simulate (i.e., rural, suburban and urban background air pollution) are kept (not industrial or traffic proximity stations). To operate such a filter, we select background stations that are classified from 1 to 7 according to Joly and Peuch (2012) classification. In addition, observations above a certain threshold are considered aberrant and removed. This threshold differs according to the pollutant and equal to 500 $\mu g.m^{-3}$ for O_3, 700 $\mu g.m^{-3}$ for NO_2, 1000 $\mu g.m^{-3}$ for PM10 and 700 $\mu g.m^{-3}$ for PM2.5.

Modelled and observed average hourly, weekly and monthly cycles of pollutant concentrations were computed per season (i.e., January-February-March, JFM; April-May-June, AMJ; July-August-September, JAS; October-November-December, OND) to assess the benefit of the corresponding temporal profiles. For each cycle, the spatial median of the temporal correlation was estimated for the hourly/monthly/daily mean and daily maximum concentrations. The primary focus is on the correlation coefficient as temporal profiles mainly influence variability. However, since the modification of temporal profiles can also impact absolute concentration values, additional metrics—Root Mean Square Error (RMSE) and Mean Bias (MB) — were computed for daily maximum and daily mean concentrations, categorized by concentration intervals. Diagnostics are provided for all individual CAMS regional models (Table 1) and the median ensemble (ENS). To automate the evaluation process, the Python package evaltools (https://opensource.umr-cnrm.fr/projects/evaltools/wiki, last accessed: March 2025) was used. This package is specifically designed to evaluate predictive models of surface atmospheric composition against in-situ observations, and it is used for the evaluation of CAMS air quality models.

2.5 Experimental setup

To assess the impact of updating emission temporal profiles on modelled concentrations, each individual CAMS model performed two annual simulations for the meteorological year 2018. Both experiments were run on a European domain (25°W-45°E, 30°N-72°N) with a 0.2ºx0.2º (SILAM, MONARCH, MINNI, CHIMERE, LOTOS-EUROS) and 0.1ºx0.1º (EMEP,

https://doi.org/10.5194/egusphere-2025-1287
Preprint. Discussion started: 11 April 2025

DEHM, EURAD-IM, MATCH, GEM-AQ and MOCAGE) horizontal resolution and using global meteorological and chemical boundary and initial conditions produced with the ECMWF Integrated Forecasting System (IFS) (Flemming et al., 2015). The simulations used the same anthropogenic (CAMS-REG-AP_v4.2 inventory for year 2017), biomass burning (GFASv1.2 for the year 2018) and other natural emissions (model-dependent). No assimilation or data fusion techniques were applied to the modelled results. In the first experiment (hereinafter referred to as expA) all models used their default set of emission temporal profiles (Table 2), while in the second experiment (hereinafter referred to as expB) they used the CAMS-REG-TEMPO_v3.2 dataset. For the year-dependent CAMS-REG-TEMPO_v3.2 profiles (Table 3), the weight factors corresponding to the year 2018 were applied.

3 Results

3.1 Emissions

Figure 1 to Figure 6 compare the monthly, weekly and hourly emission temporal distributions for key pollutants (i.e., NOx, NMVOC, SOx, NH_3, PM_{10}, $PM_{2.5}$) across different sectors at the EU27 plus UK and Norway level using the CAMS-REG-TEMPO_v3.2, TNO and GENEMIS profiles. These distributions were obtained by applying each temporal profile dataset to the CAMS-REG-AP_v4.2 emissions. Since the total annual emissions remain the same in all three cases, the comparison focuses on differences in temporal allocation. Relative differences [%] in emission distributions— CAMS-REG-TEMPO vs. TNO and CAMS-REG-TEMPO vs. GENEMIS—are summarized per pollutant by month-of-the-year, day-of-the-week and hour-of-the-day are summarised in the Supplementary Material (Figures S1 to S3). For hourly emission cycles, we excluded GENEMIS from the analysis, as they report the exact same hourly profiles as TNO. Instead, an additional dataset was included in the comparison: the default hourly temporal factors used in EMEP and CHIMERE, which combine GENEMIS hourly profiles (identical to TNO profiles) with the road transport profiles from Menut et al., (2012). We refer to this dataset as GENEMIS-Menuetal2012.

3.1.1 Monthly emission cycles

The seasonality of NO_x emissions is mainly dominated by the road transport and industry sectors (energy and manufacturing) (Fig. 1). The monthly cycles obtained with the three temporal profile databases are generally similar, with differences ranging between -10 and 10% depending on the month (Fig. S1). CAMS-REG-TEMPO presents larger emissions in February, March, July, August and November compared to the other datasets. The differences in July and August are mainly attributed to the off-road transport sector (GNFR_I, included in the "Others" category), which CAMS-REG-TEMPO assumes to increase during summer, whereas TNO and GENEMIS use flat profiles. In February, March and November, the differences are mainly related to the meteorology-dependent profiles used in CAMS-REG-TEMPO for diesel exhaust road transport (GNFR_F2) and residential/commercial combustion (GNFR_C). These profiles result in a stronger contrast between cold and warm months, leading to higher emissions during colder periods compared to the static profiles used in TNO and GENEMIS.

https://doi.org/10.5194/egusphere-2025-1287
Preprint. Discussion started: 11 April 2025

For NMVOC (Fig. 1 and Fig. S1), the differences in monthly emissions between CAMS-REG-TEMPO and TNO are also relatively small (ranging between -10% and 10%). This similarity is partly due to both datasets using the same monthly profile for the solvents sector (GNFR_E). However, larger discrepancies are observed when comparing CAMS-REG-TEMPO and GENEMIS, with the former reporting significantly lower emissions in spring —up to 20% lower in April (Fig. S1). This discrepancy is mainly driven by the different monthly profiles considered for the agricultural waste burning emissions, which fall under the GNFR_L category.

For SO_x, the monthly emission cycles are largely dominated by the industry sector (Fig. 1). Compared to winter, the drop in industrial emissions during summer and fall is less pronounced in CAMS-REG-TEMPO than in other datasets. Consequently, emissions in July and August are up to 20% higher compared to those obtained derived using GENEMIS profiles (Fig. S1). Conversely, emissions in January and December tend to be lower with CAMS-REG-TEMPO, showing reduction of -5% compared to TNO and -8% compared to GENEMIS.

NH_3 exhibits the largest differences in monthly emission distributions, especially when comparing CAMS-REG-TEMPO and TNO profiles (Fig. 2). CAMS-REG-TEMPO reports a distinct bi-modal seasonality, with a primary peak in April, mainly driven by fertilizer emissions (GNFR_L), and a second lower-intensity peak in June, mainly linked to livestock emissions (GNFR_K). In contrast, the TNO profile allocates the majority of NH_3 emissions to March. Using CAMS-REG-TEMPO instead of TNO leads to a decrease in emissions by more than -50% during that month and an increase above 100% in summer (Fig. S1). The GENEMIS profile is more in line with that of CAMS-REG-TEMPO, but with a flatter distribution, allocating more emissions in winter and fewer in summer (Fig. S1). It is worth mentioning that the seasonality reported by CAMS-REG-TEMPO is well aligned with European NH_3 emission monthly patterns derived from satellite observations, as recently reported by Ding et al., (2024).

For PM_{10}, all three temporal profile datasets allocate more emissions in winter than in summer, mainly due to the seasonality of residential and commercial combustion emissions (GNFR_C). These emissions increase during cold months as combustion activities for space heating intensify. CAMS-REG-TEMPO allocates more emissions in January and February compared to TNO (up to +20% in February), while its estimates for these months are closely aligned with GENEMIS (differences below -5%). In November and December, CAMS-REG-TEMPO reports between 15% and 20% more PM10 emissions than TNO and GENEMIS, respectively. This discrepancy mainly comes from differences in the monthly allocation of agricultural waste management emissions (GNFR_L) across datasets. In CAMS-REG-TEMPO, these emissions peak between October and December, whereas GENEMIS assigns them between September and November. TNO, on the other hand, distributes them across two peaks of similar intensity—one in spring (March-April) and another in summer (July-August).

https://doi.org/10.5194/egusphere-2025-1287
Preprint. Discussion started: 11 April 2025

For $PM_{2.5}$, the monthly cycles obtained with CAMS-REG-TEMPO and GENEMIS present a U-shape pattern, whereas TNO shows a V-shape trend (Fig. 2 and Fig. S1). This discrepancy arises from differences in the monthly profiles for residential and commercial combustion emissions. The CAMS-REG-TEMPO and GENEMIS profiles are similar, as both consider the impact of meteorology (i.e., temperature-driven variations in heating demand). Maximum differences occur in February, where when CAMS-REG-TEMPO reports 20% higher emissions than TNO, and in July, where CAMS-REG-TEMPO reports 20% more emissions than GENEMIS (Fig. S1). Additionally, CAMS-REG-TEMPO shows a pronounced drop in residential and commercial combustion emissions between winter and spring, leading to lower total PM2.5 emissions compared to both TNO (-20%) and GENEMIS (-25%).

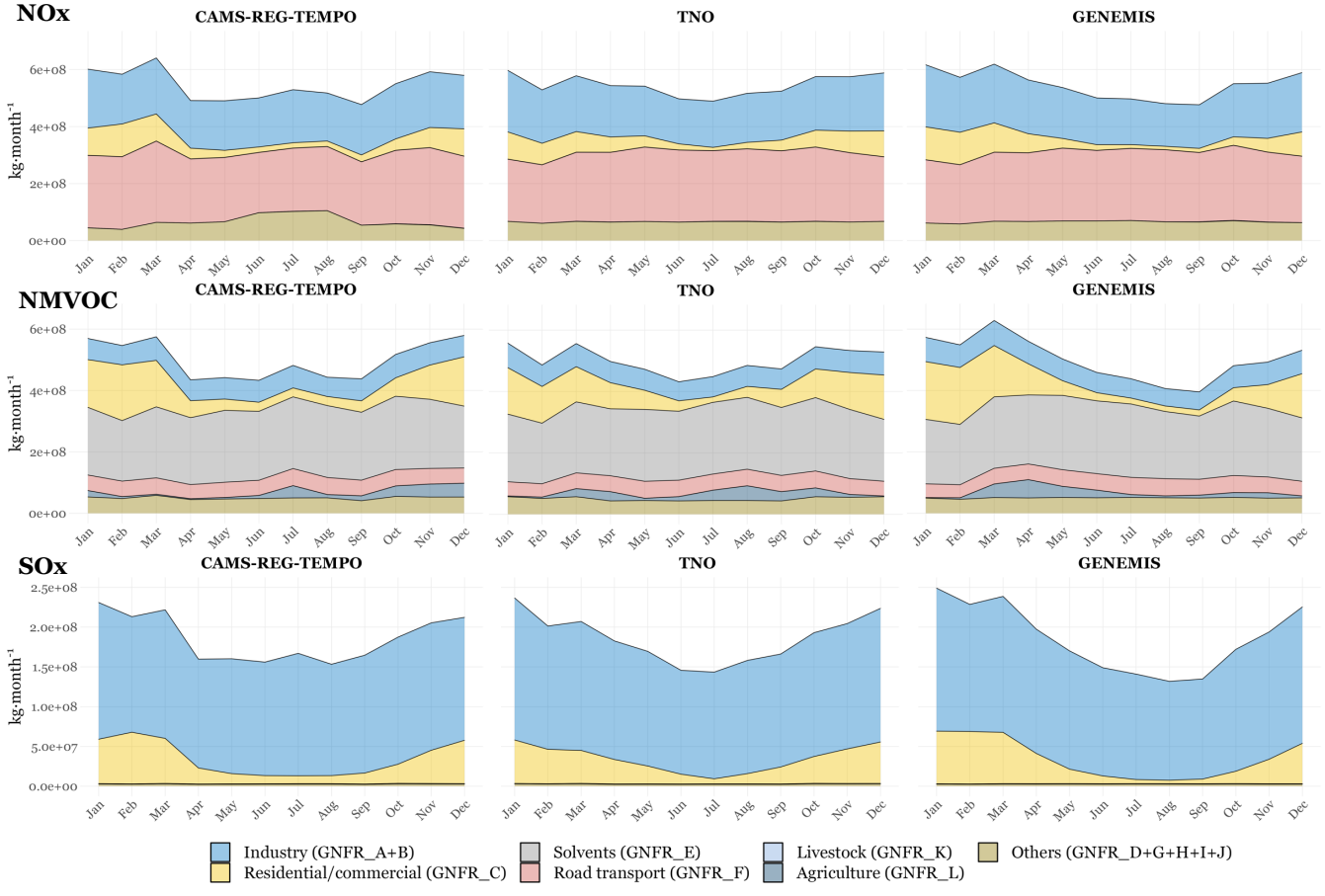

Figure 1 Monthly NO_x, NMVOC and SO_x emission temporal distributions obtained per pollutant and sector at the EU27 plus UK and Norway level when using the CAMS-REG-TEMPO, TNO and GENEMIS profiles, respectively.

https://doi.org/10.5194/egusphere-2025-1287
Preprint. Discussion started: 11 April 2025

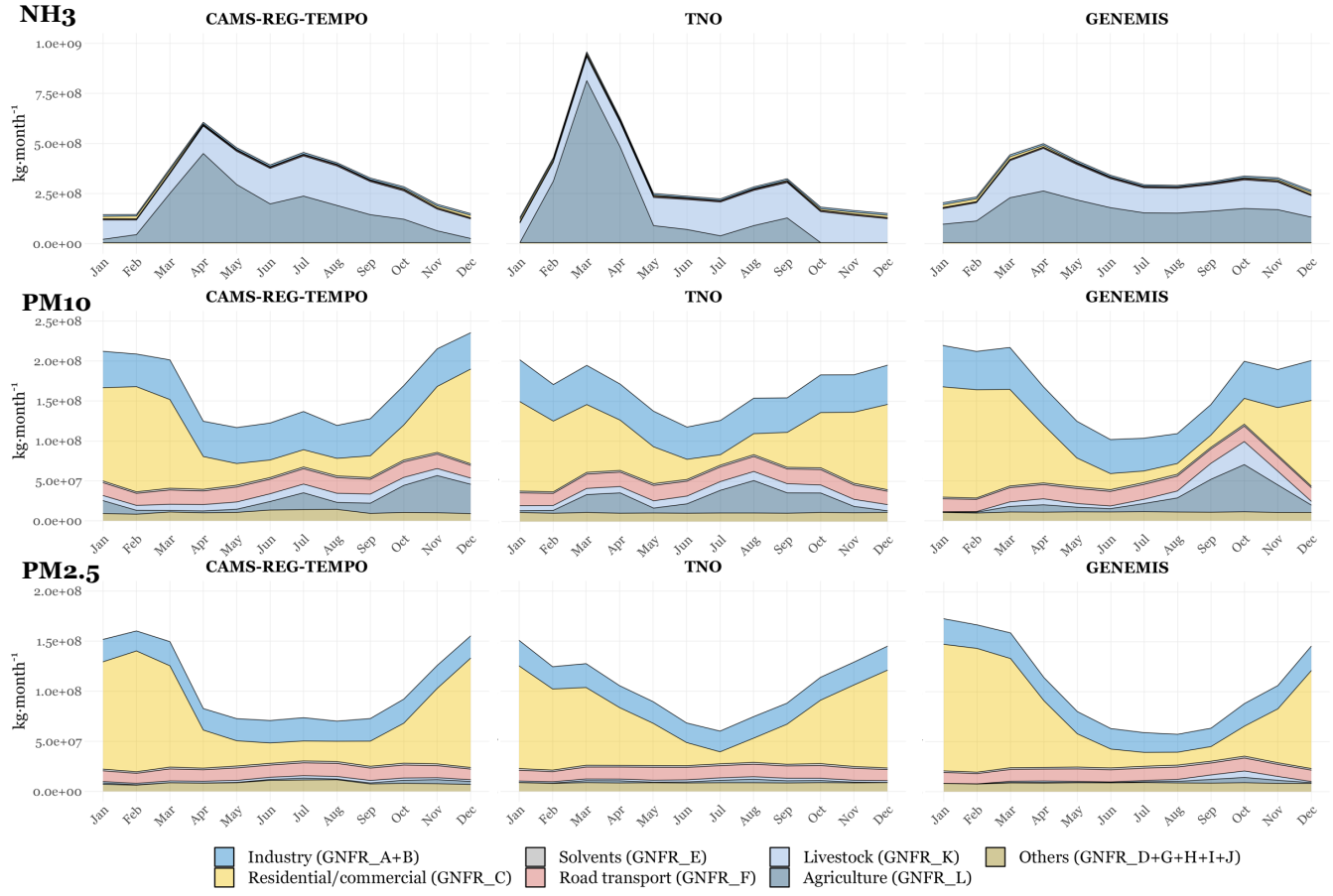

Figure 2 Same as Fig. 1 for NH_3, PM_{10} and $PM_{2.5}$

300

https://doi.org/10.5194/egusphere-2025-1287
Preprint. Discussion started: 11 April 2025

3.1.2 Weekly emission cycles

The NO_x weekly cycle obtained with CAMS-REG-TEMPO presents a significantly larger drop of emissions between weekdays and weekends compared to TNO and GENEMIS (Fig. 3). As a result, Saturday and Sunday emissions in CAMS-REG-TEMPO are 11% and 21% lower than those obtained using the TNO profiles (Fig. S2). The differences are slightly larger when compared to GENEMIS (-18% on Saturday and -25% on Sunday). Conversely, emissions during weekdays are between 5% and 10% higher with CAMS-REG-TEMPO than with the other datasets. These discrepancies are mainly driven by differences in the weekly profiles for road transport and, to a lower extent, for off-road transport (included in the "Others" category).

For NMVOC, the weekly distributions in CAMS-REG-TEMPO and TNO are nearly identical, with differences ranging between -2% and 2%, depending on the day of the week (Fig. 3 and Fig. S2). However, the discrepancies are larger when comparing CAMS-REG-TEMPO and GENEMIS, with the former reporting 12.5% lower emissions on Saturdays and 10% higher emissions on Sundays. These differences are linked variations in the weekly profiles for the solvent use sector. Both CAMS-REG-TEMPO and TNO solvent use emissions experience a sharp drop between Friday and Saturday, followed by stable emissions throughout the weekend. In contrast, GENEMIS presents a gradual decline between Friday and Sunday.

The SO_2 weekly cycles in CAMS-REG-TEMPO and GENEMIS are almost identical, both showing a very slight drop in emissions over weekends compared to weekdays (Fig. 3). The TNO profile shows a more pronounced weekend drop, with CAMS-REG-TEMPO reporting 6% higher emissions on Saturdays and 4% higher on Sundays compared to TNO. (Fig. S2).

Unlike the large discrepancies observed in NH_3 monthly cycles, the weekly cycles reported by CAMS-REG-TEMPO, TNO and GENEMIS for this species are almost identical (Fig. 3), with all three datasets assuming a near-flat weekly distribution of emissions.

For PM10 and PM2.5, similar discrepancies are observed across datasets (Fig. 3). Compared to TNO, CAMS-REG-TEMPO reports slightly lower emissions on weekdays (up to -2.5%) and higher emissions on weekends (up to 7.5%) (Fig. S2). Conversely, when compared to GEMINIS, CAMS-REG-TEMPO shows higher weekday emissions (up to 4%) and lower weekend emissions (up to -7.5%). For both pollutants, these differences are mainly driven variations in the weekly profiles for the residential and commercial combustion activities (GNFR_C) across the datasets.

https://doi.org/10.5194/egusphere-2025-1287
Preprint. Discussion started: 11 April 2025

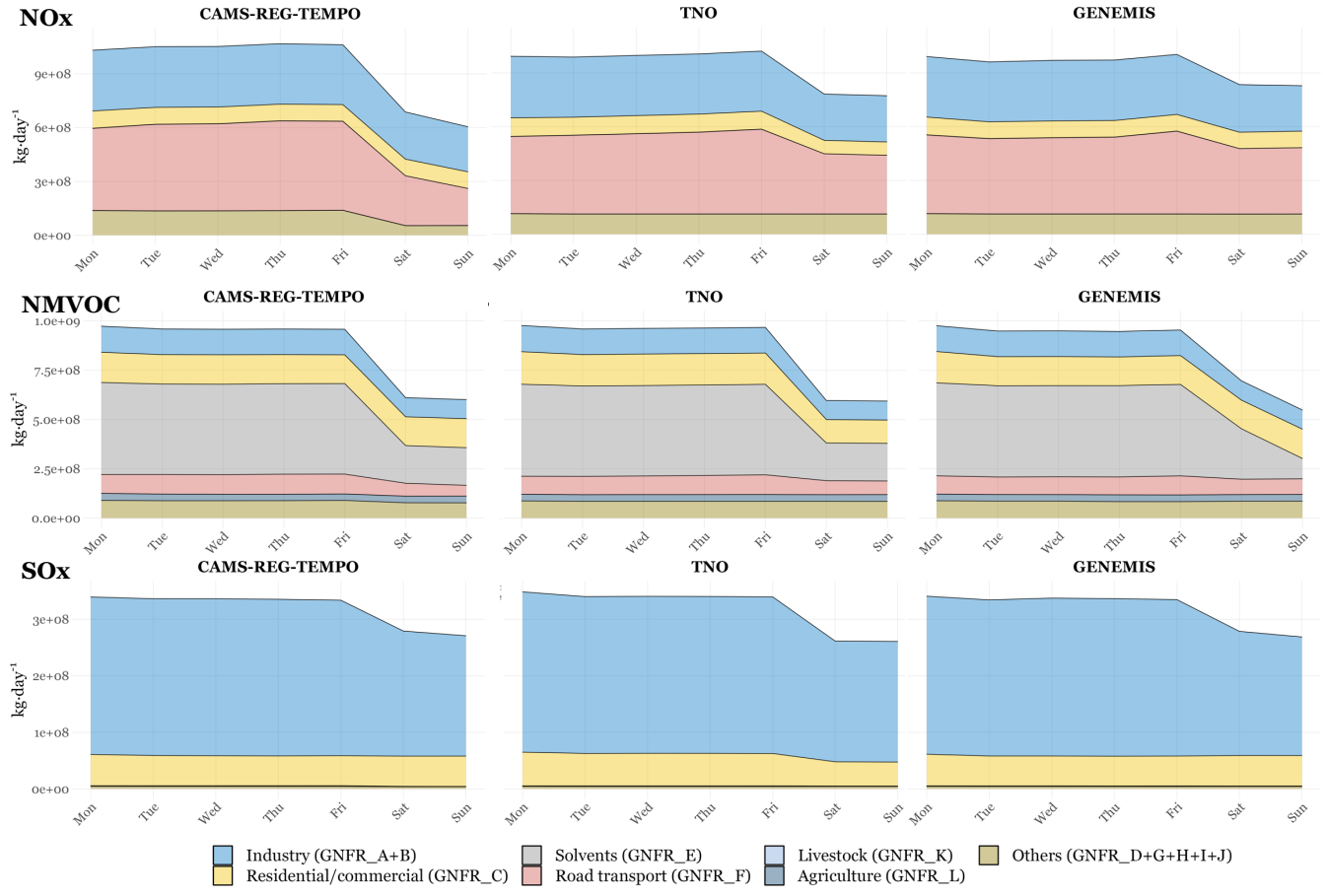

Figure 3 Weekly NO_x, NMVOC and SO_x emission temporal distributions obtained per pollutant and sector at the EU27 plus UK and Norway level when using the CAMS-REG-TEMPO, TNO and GENEMIS profiles, respectively.

335

https://doi.org/10.5194/egusphere-2025-1287
Preprint. Discussion started: 11 April 2025

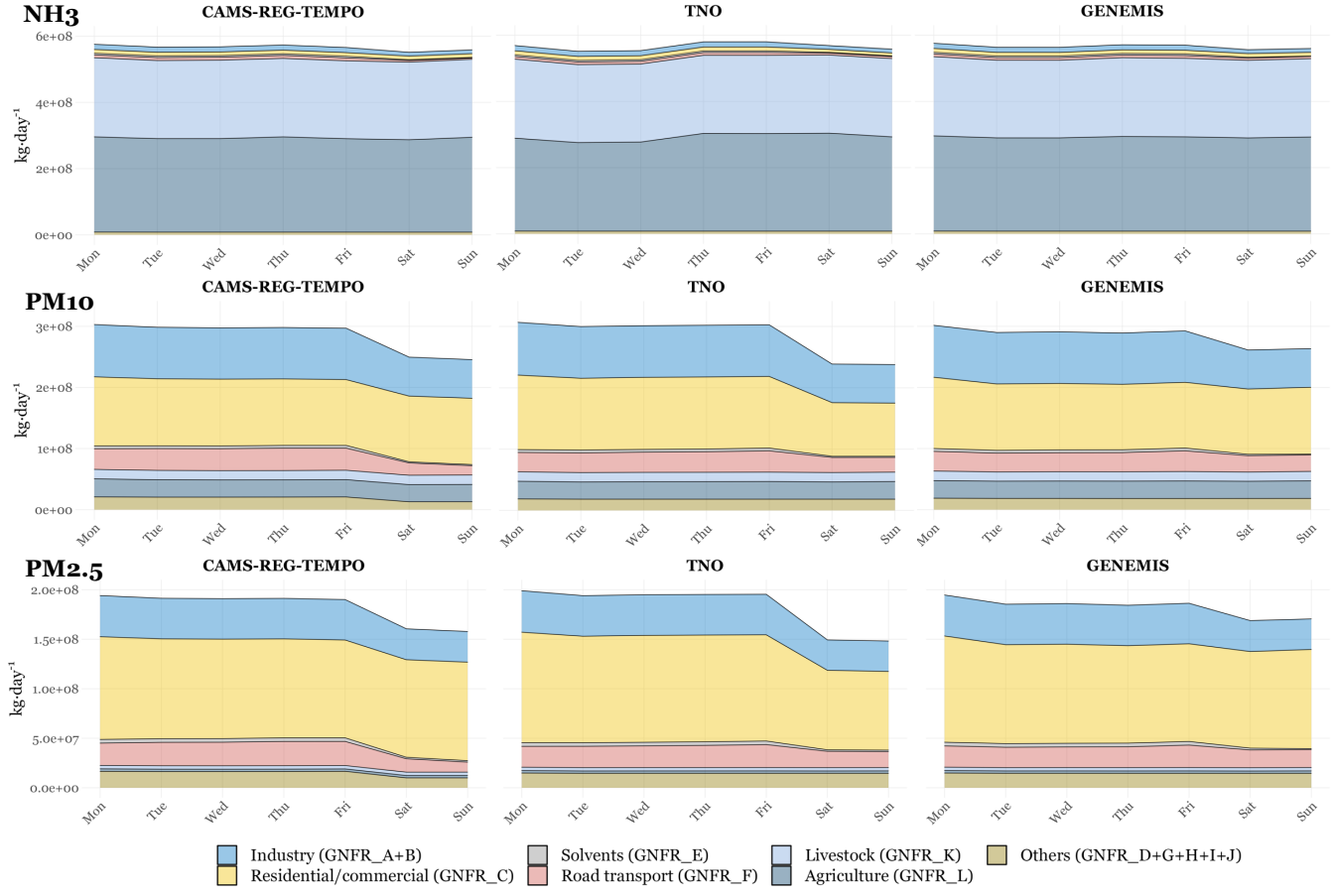

Figure 4 Same as Fig. 3 for NH_3, PM_{10} and $PM_{2.5}$

340

https://doi.org/10.5194/egusphere-2025-1287
Preprint. Discussion started: 11 April 2025

3.1.3 Hourly emission cycles

The NO_x hourly distributions obtained with CAMS-REG-TEMPO, TNO and GENEMIS-Menutetal2012 profiles all present a morning and afternoon peak, mainly driven by the diurnal variation of road transport emissions (Fig. 5). However, the timing and intensity of these peaks vary significantly across datasets, especially when comparing CAMS-REG-TEMPO with GENEMIS-Menutetal2012. Morning peak is much more pronounced in CAMS-REG-TEMPO, with total NO_x emissions being approximately 25% higher at 07:00 and 08:00h local time (LT) compared to GENEMIS-Menutetal2012 (Fig. S3). For the afternoon peak, significant differences exist in both intensity and timing. In CAMS-REG-TEMPO, the peak occurs between 17:00 and 18:00 LT, whereas in GENEMIS-Menutetal2012, emissions increase more gradually and peak later, between 19:00 and 20:00 LT. Consequently, NO_x emissions in CAMS-REG-TEMPO are 30-45% higher than in GENEMIS-Menutetal2012 during 17:00h-18:00h LT. Conversely, night-time NO_x emissions in CAMS-REG-TEMPO are between 30 and 50% lower than in GENEMIS-Menutetal2012. The main reason behind these large discrepancies is in the design of the road transport profiles. While CAMS-REG-TEMPO were constructed considering traffic congestion statistics (see Sect. 2.3.2), in GENEMIS-Menutetal2012 profiles rely on measured NO_2 concentrations in urban traffic stations, which diurnal variation is controlled not only by road transport emissions but also by other physical and chemical processes not related to traffic activity, such as boundary layer dynamics and NOx titration (Li et al., 2021). The comparison between CAMS-REG-TEMPO and TNO highlights smaller discrepancies in peak intensity and timing. While both datasets show similar peak structures, CAMS-REG-TEMPO reports slightly higher emissions, with morning peak emissions (~07:00–08:00 LT) being 5% higher than those in TNO. Nighttime NO_x emissions are about 15% lower in CAMS-REG-TEMPO compared to TNO, mainly due to differences in off-road transport sector assumptions: while TNO proposes a flat profile, CAMS-REG-TEMPO concentrates most off-road emissions during daytime.

For NMVOC (Fig. 5), a pattern similar to that observed for NO_x emissions emerges, with CAMS-REG-TEMPO allocating less emissions during night-time (between -5% and -20%) and more during daytime (between 5% and 10% (Fig. S3). However, differences are less pronounced than for NO_x as all three datasets consider the same hourly profile for the dominant sector — solvent use (GNFR_E). The higher emissions in CAMS-REG-TEMPO during daytime is mainly linked to three factors; first, off-road transport emissions increase during daytime; second, the diurnal distribution of gasoline evaporative emissions (GNFR_F4, included in the “road transport” category) peaks around noon due to the influence of temperature; and third, the hourly profile for agricultural waste burning emissions peaks around noon.

For SO_x (Fig. 5), differences in hourly emission cycles are rather small. CAMS-REG-TEMPO shows a flatter distribution of industrial emissions, resulting in smaller contrasts between nigh-time and day-time levels. Consequently, CAMS-REG-TEMPO reports lower SO_x emissions during daytime (less than -5% between 07:00 and 17:00h LT) and higher emissions

https://doi.org/10.5194/egusphere-2025-1287
Preprint. Discussion started: 11 April 2025

during nighttime (between 2% and 8% from 18:00 till 06:00h LT) compared to both the TNO and GENEMIS-Menutetal2012 profiles (Fig. S3).

Similar to SO_x, differences in NH_3 diurnal cycles are minimal (<5%, Fig. 6 and Fig. S3), as all three datasets consider the same hourly profiles for agriculture and livestock emissions, the two dominant sources of NH_3.

Finally, large discrepancies are observed in the diurnal distributions of PM10 and PM2.5 (Fig. 6). CAMS-REG-TEMPO reports much higher emissions during the evening hours (17:00- 22:00h LT). This discrepancy is mainly driven by differences in the hourly distribution of residential and commercial combustion emissions (GNFR_C). In CAMS-REG-TEMPO, these emissions, largely linked to residential wood combustion in fireplaces, boilers and other types of appliances, are assumed to peak in the evening. In contrast, TNO and GENEMIS-Menutetal2012 distribute emissions more evenly, with two peaks: one in the morning and another in the afternoon. Consequently, PM emissions in CAMS-REG-TEMPO are over 50% higher than those in TNO and GENEMIS-Menutetal2012 between 17:00 and 19:00h LT, while morning peak emissions are approximately 40% lower.

https://doi.org/10.5194/egusphere-2025-1287
Preprint. Discussion started: 11 April 2025

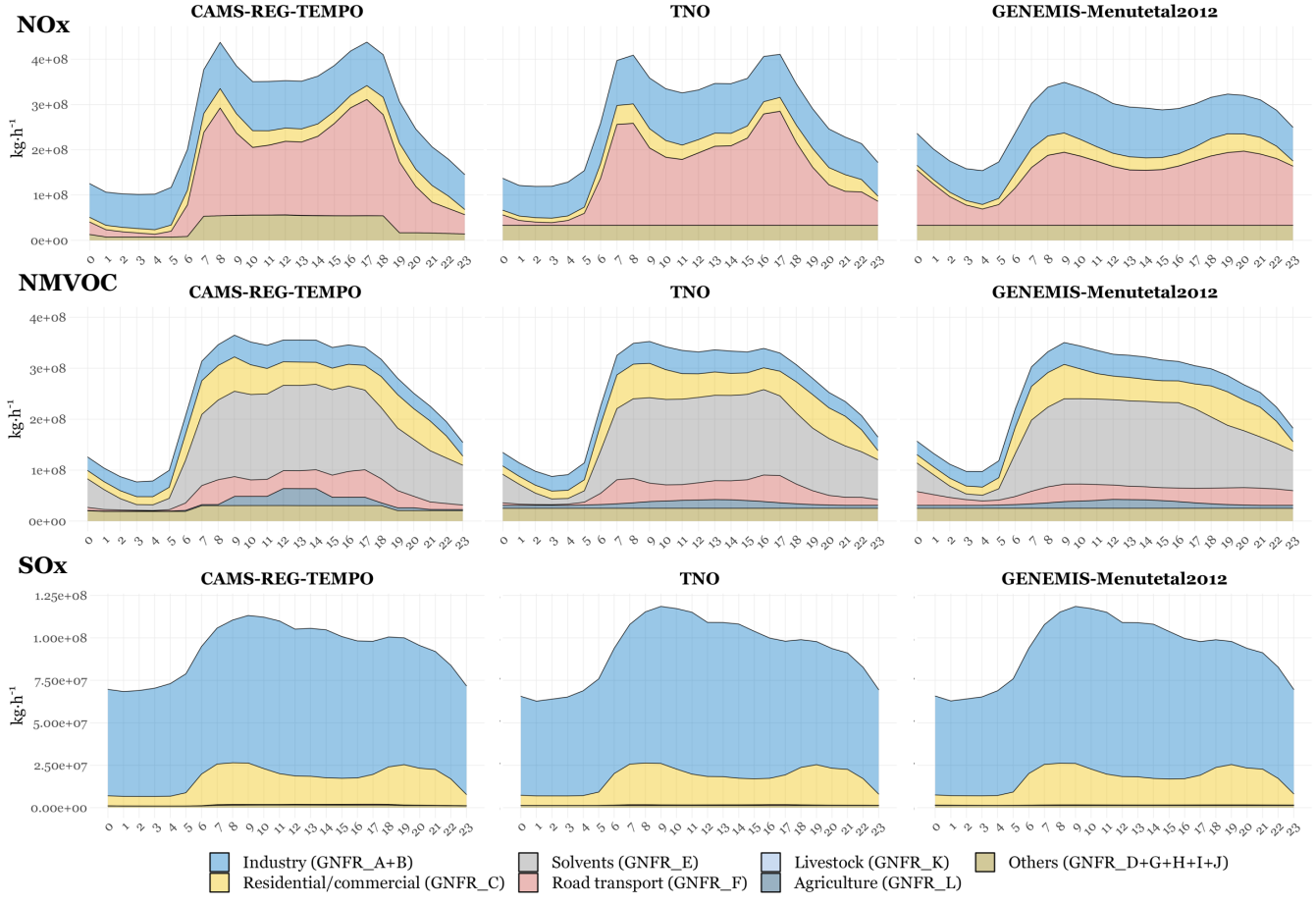

Figure 5 Diurnal NO_x, NMVOC and SO_x emission temporal distributions obtained per pollutant and sector at the EU27 plus UK and Norway level when using the CAMS-REG-TEMPO, TNO and GENEMIS profiles, respectively.

https://doi.org/10.5194/egusphere-2025-1287
Preprint. Discussion started: 11 April 2025

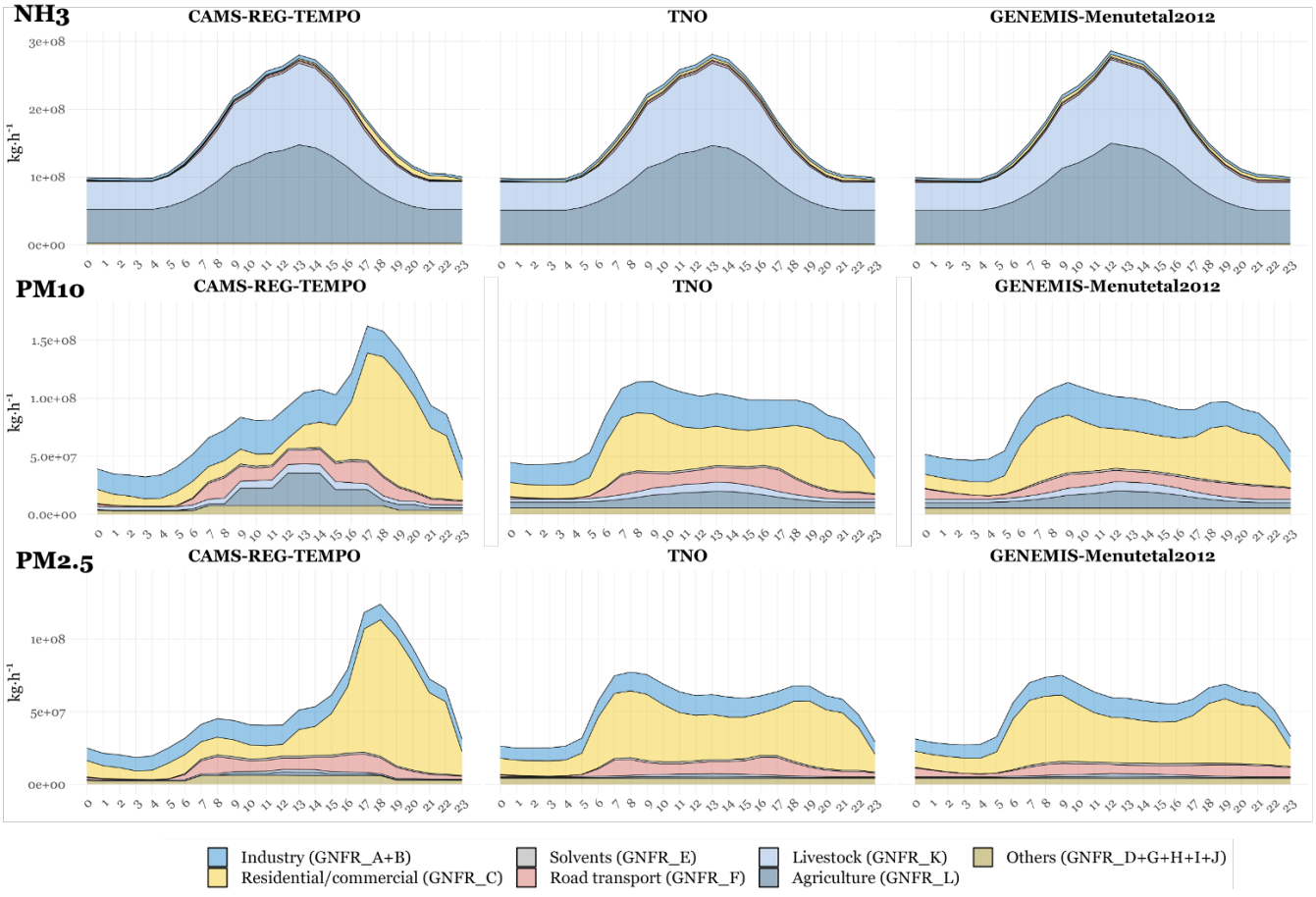

Figure 6 Same as Fig. 5 for NH_3, PM_{10} and $PM_{2.5}$

395

https://doi.org/10.5194/egusphere-2025-1287
Preprint. Discussion started: 11 April 2025

3.2 Correlation of modelled diurnal, weekly and monthly cycle concentrations with surface observations

Figure 7 summarises the differences in temporal correlation values obtained by the ENS in expB (CAMS-REG-TEMPO_v3.2 profiles) and expA (default profiles). Results are provided per species, cycle type (monthly, weekly and diurnal) and season. Positive values indicate improvements in correlation when using CAMS-REG-TEMPO, while negative values (red boxes) indicate degradations. Absolute changes in correlation between -0.01 and 0.01 are considered insignificant (grey boxes). The values in brackets indicate the maximum and minimum correlation differences obtained across the individual CAMS regional models. Results for each individual model are provided in the Supplementary Material (Fig. S4). Note that for DEHM (MATCH) NO_2 and O_3 (PM_{10} and $PM_{2.5}$) modelled results could not be provided and were excluded from the analysis.

O_3 is the pollutant with the lowest sensitivity to changes in temporal profiles. For both monthly and diurnal cycles (all seasons), correlation values remain almost unchanged when moving from the default (TNO, GENEMIS) to CAMS-REG-TEMPO profiles. Note that for these two cycles the correlation values of the ENS are also the largest among the four species analysed (between 0.90 and 0.95, see Sect. 3.2.2 for more details) and therefore the room for improvement is very limited. At the weekly level, the impact varies by season. During JFM and OND, slight correlation improvements are observed (+0.03 and +0.02), whereas during AMJ and JAS, degradations of -0.1 and -0.03, respectively, are reported. These degradations clearly contrast with the improvements in NO_2 weekly cycles observed during the same seasons (+0.13 for AMJ and +0.08 for JAS).

NO_2 exhibits the largest variation in temporal correlation due to CAMS-REG-TEMPO, with only minor degradations occurring in the diurnal cycle during AMJ (-0.03). The improvements in NO_2 weekly correlations are consistent across all models except one, with differences between expB and expA reaching up to +1.0 (see Sect. 3.2.1 for more details).

For PM_{10}, the major improvement occurs in the OND diurnal cycle (+0.13), the JFM diurnal and JAS weekly cycles also showing a slight improvement (+0.02 in both cases), while a minor degradation is reported for the AMJ weekly cycle (-0.03). PM_{10} is also the only pollutant to show a slight improvement in the monthly cycle correlation (+0.02), while other pollutants showing no changes.

Similarly, $PM_{2.5}$ shows a major correlation improvement in the OND diurnal cycle (+0.15), mirroring PM_{10}. The OND weekly cycle shows a slight improvement (+0.02), while for other seasons correlation values remain either unchanged (monthly and all weekly cycles except AMJ) or show slightly degradations (JFM and AMJ diurnal cycles: -0.02; AMJ weekly cycle: -0.04).

Overall, the sensitivity to changes in the emission temporal profiles is larger for NO_2 and PM_{10}, which are dominated by primary sources, and lower for $PM_{2.5}$ and O_3, which are primarily driven by secondary formation and, in the case of O_3, by remote influences due to its higher lifetime.

https://doi.org/10.5194/egusphere-2025-1287
Preprint. Discussion started: 11 April 2025

pollutant	diurnal				weekly				monthly
	JFM	AMJ	JAS	OND	JFM	AMJ	JAS	OND	
O_3	0.00 (-0.04 / 0.02)	0.00 (-0.02 / 0.02)	0.00 (-0.01 / 0.02)	0.00 (-0.04 / 0.02)	0.03 (0.00 / 0.03)	-0.10 (-0.13 / -0.02)	-0.03 (-0.04 / 0.01)	0.02 (-0.03 / 0.09)	0.00 (-0.03 / 0.00)
NO_2	0.05 (-0.10 / 0.19)	-0.03 (-0.18 / 0.1)	0.00 (-0.15/ 0.07)	0.07 (-0.11 / 0.24)	0.16 (-0.09 / 0.44)	0.13 (0.01 / 1.0)	0.08 (0.01 / 0.76)	0.06 (-0.08 / 0.17)	0.00 (-0.01 / 0.1)
PM_{10}	0.02 (-0.01 / 0.32)	-0.01 (-0.2 / 0.02)	0.01 (-0.07 / 0.06)	0.13 (0.04 / 0.29)	0.01 (-0.03 / 0.07)	-0.03 (-0.07 / 0.03)	0.02 (-0.01 / 0.17)	0.00 (-0.02 / 0.03)	0.02 (-0.08 / 0.07)
$PM_{2.5}$	-0.02 (-0.08 / 0.49)	-0.02 (-0.36 / 0.02)	-0.01 (-0.13 / 0.11)	0.15 (0.03 / 0.51)	0.00 (-0.08 / 0.06)	-0.04 (-0.13 / 0.02)	0.00 (-0.01 / 0.1)	0.02 (-0.03 / 0.04)	0.00 (-0.09 / 0.1)

Figure 7 Summary of the ENS correlation differences (expB – expA) per species (O_3, NO_2, PM_{10}, $PM_{2.5}$), season (JFM, AMJ, JAS, OND) and cycle (diurnal, weekly, monthly). Values between brackets indicate the minimum and maximum correlation differences among the individual CAMS regional models. Boxes highlighted in green/orange/grey indicate an improvement/degradation/no significant changes (between -0.01 and 0.01) in the correlation when using CAMS-REG-TEMPO.

Figure 8 illustrates the ENS correlation differences (expB – expA) at the station level, categorized by species (O_3, NO_2, PM_{10}, $PM_{2.5}$) and selected seasons. Each species is analysed during the season when its concentrations are at their maximum levels. For NO_2 a general improvement in correlation during JFM is observed across the domain. In contrasts, O_3 during JAS shows more heterogeneous results, with improvements in central Europe (e.g., Germany) and degradations in western (e.g. Spain, France) and eastern (e.g. Poland) countries. Interestingly, stations near large urban areas tend to show correlation improvements. Downwind urban areas other processes like meteorology and photochemistry may dominate the signal. For PM_{10}, JFM correlations improve at stations in Germany, Poland, Portugal and parts of Spain, whereas degradations are observed in France and the Czech Republic. Conversely, for $PM_{2.5}$ during OND, France reports more stations with improved correlations, while Germany exhibits a decrease in most sites.

https://doi.org/10.5194/egusphere-2025-1287
Preprint. Discussion started: 11 April 2025

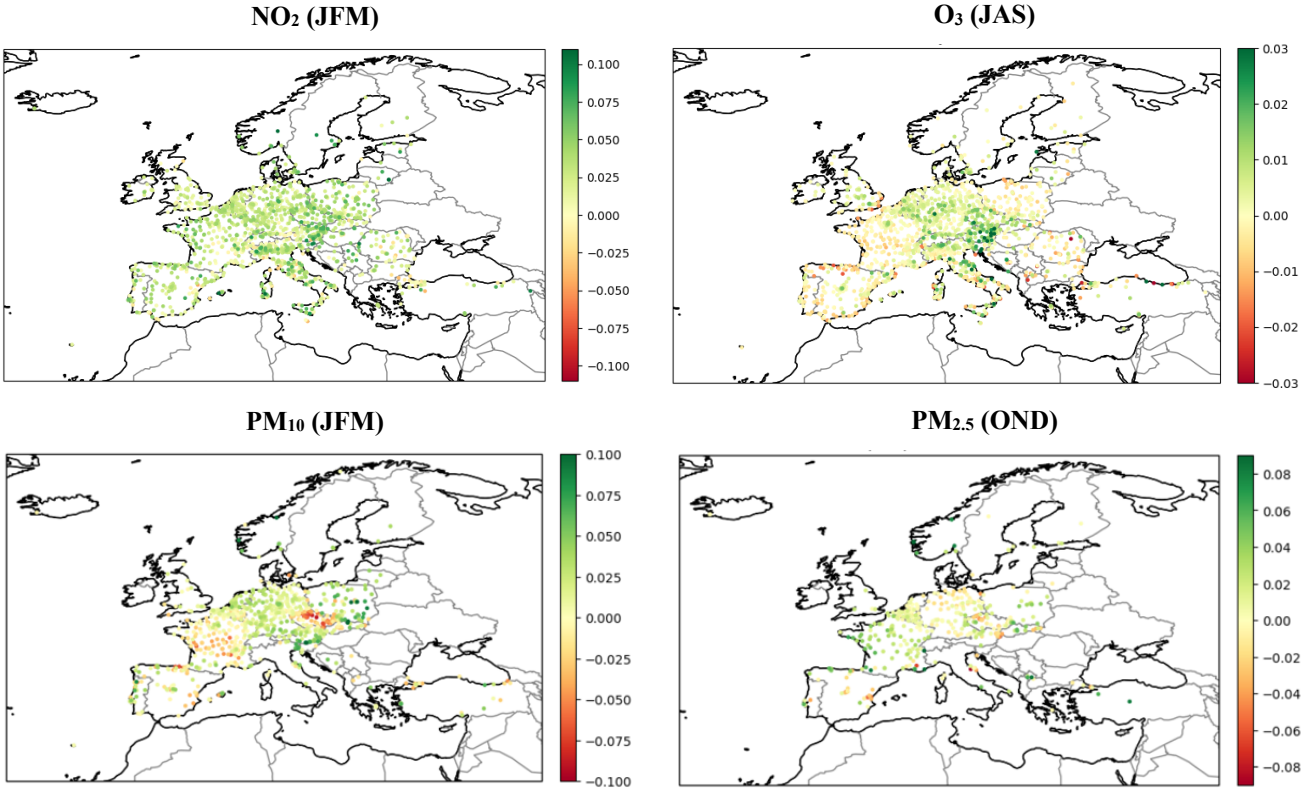

Figure 8 Summary of the ENS correlation differences (expB – expA) at the station level per species (O_3, NO_2, PM_{10}, $PM_{2.5}$) and selected seasons. Green values indicate an improvement in the correlations when using CAMS-REG-TEMPO, while red values indicate a degradation.

450

https://doi.org/10.5194/egusphere-2025-1287
Preprint. Discussion started: 11 April 2025

3.2.1 NO_2

There is no significant variation in the ENS correlation coefficient for the NO_2 monthly cycle when using CAMS-REG-TEMPO (0.83 versus 0.84). However, its implementation induces a consistent positive response across most individual models, with correlation increases ranging from +0.09 (CHIMERE) to +0.004 (EMEP) (Fig. 9). Notably, the ENS captures better the observed NO_2 peak in February (Fig. 9). This improvement is likely driven by the meteorology-dependent temporal profiles applied to the residential and commercial combustion and diesel road transport sectors in CAMS-REG-TEMPO. These profiles lead to increases emissions during February, reflecting the Hartmut cold spell, which impact Europe during that month (C3S, 2018).

The largest improvement in NO_2 correlation is observed in the weekly cycle across all models (Fig. 10). For the ENS, correlation increases from 0.66 to 0.82 (+0.16) in JFM, 0.66 to 0.80 (+0.14) in AMJ, 0.78 to 0.86 (+0.08) in JAS and 0.82 to 0.88 (+0.06) in OND, exceeding 0.8 for all four seasons. This improvement is consistent across all individual models except for MATCH in JFM and OND. The effect is especially pronounced in models that previously used GENEMIS profiles in the expA (i.e., EMEP and CHIMERE), showing substantial correlation increases —up to +1.00 in AMJ (from -0.21 to 0.79) and +0.76 in JAS (from 0.10 to 0.86). The ENS improvement is mainly due to a better reproduction of the observed weekday-to-weekend drop in NO_2 concentrations when using CAMS-REG-TEMPO. As discussed in Sect. 3.1.2, the TomTom congestion-derived profiles used in CAMS-REG-TEMPO for the road transport sector result in larger weekday-to-weekend differences in NO_x emissions, particularly compared to the GENEMIS profiles.

For the NO_2 diurnal cycle, results vary considerably depending on the model and season (Fig. 11). In expA, correlation values for the ENS range between 0.64 to 0.75. A slight positive impact is observed for the ENS and most of CAMS individual models during JFM and OND (+0.05 and +0.07 for the ENS, respectively), when NO_2 levels are at their maximum, while no changes are observed during JAS. Conversely, a slight degradation occurs during AMJ (-0.03), mainly due to changes in the intensity of the morning (6-8 a.m.) and evening (6-8 p.m.) peaks in the diurnal cycle. It is important to note that the temporal emission profiles in expA are not uniform across all models (Table 2), which partly explains the heterogeneous results. However, even among models using the same profiles in expA, contrasting results emerge when switching to CAMS-REG-TEMPO profiles. For instance, while MONARCH and MINNI show consistent improvements across all four seasons (correlation values increasing from +0.02 to +0.20), LOTOS-EUROS correlations are consistently degraded (decreases from -0.02 to -0.23), despite all three models using TNO profiles in expA. Similarly, while CHIMERE shows significant correlation improvements in all seasons ranging from +0.06 in AMJ and +0.24 in OND, EMEP reports only slight improvements in JMF (+0.04) and OND (+0.03), even though both models use the GENEMIS profiles in expA. This heterogenous impact illustrates the complex interactions between emission temporal distributions and other model-related processes, such as the planetary boundary layer depth cycle.

https://doi.org/10.5194/egusphere-2025-1287
Preprint. Discussion started: 11 April 2025

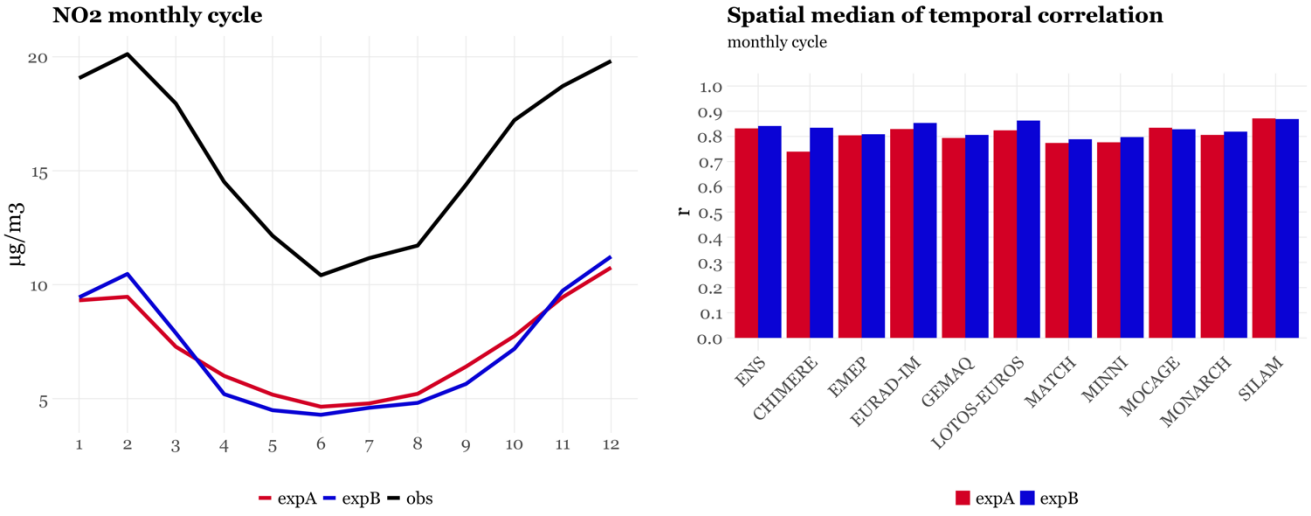

485 **Figure 9 Comparison between the observed and modelled NO_2 monthly cycle for the ENS (left) and spatial median of the temporal correlations obtained for the ENS and each individual CAMS model in expA (red) and expB (blue).**

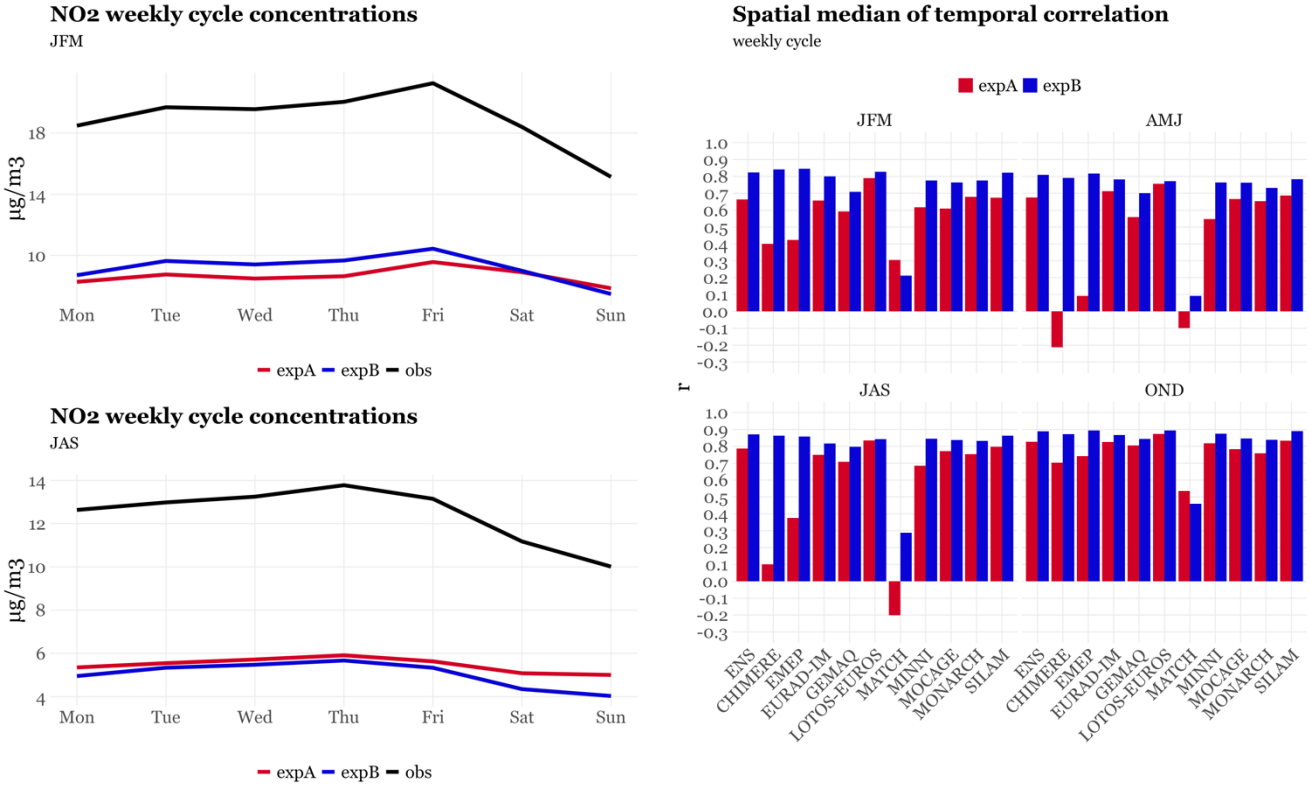

Figure 10 Comparison between the observed and modelled NO_2 weekly cycle for the ENS for JFM and JAS (left) and spatial median of the temporal correlations obtained for the ENS and each individual CAMS model per season in expA (red) and expB (blue).

https://doi.org/10.5194/egusphere-2025-1287
Preprint. Discussion started: 11 April 2025

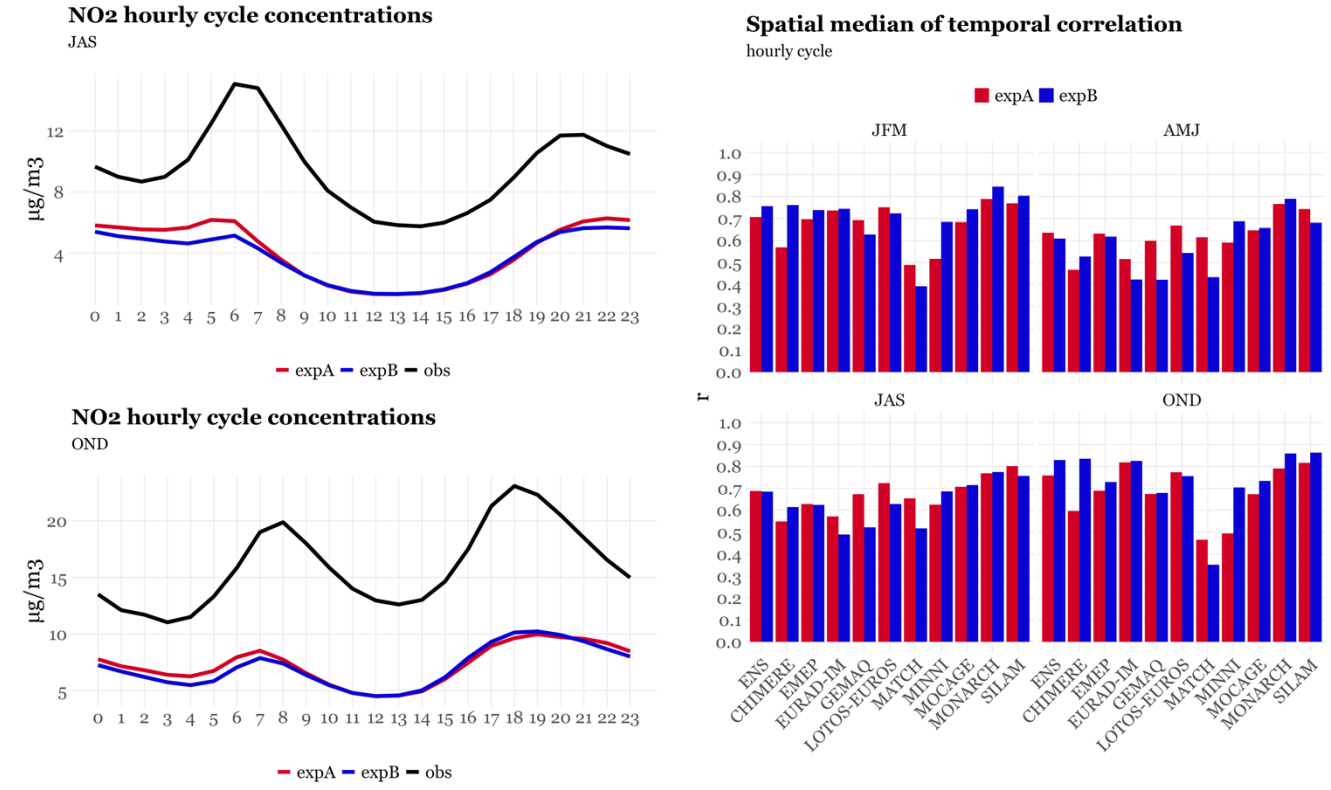

490 **Figure 11 Comparison between the observed and modelled NO_2 diurnal cycle for the ENS (UTC time) for JAS and OND (left) and spatial median of the temporal correlations obtained for the ENS and each individual CAMS model per season in expA (red) and expB (blue).**

https://doi.org/10.5194/egusphere-2025-1287
Preprint. Discussion started: 11 April 2025

3.2.2 O_3

For the ENS and most individual models, the correlation coefficient of the O_3 monthly cycle is already high (above 0.8) and shows little sensitivity to the implementation of the CAMS-REG-TEMPO profiles (Fig. 12). In contrast, the weekly cycle is impacted (Fig. 13). On average, slight correlation improvements are observed for JFM (+0.03 for the ENS) and OND (+0.02), while decreases occur in AMJ (-0.10) and JAS (-0.03). This behaviour is generally consistent across most individual models. During JFM, the use of CAMS-REG-TEMPO enhances the models' ability to capture the O_3 weekend effect —increase of O_3 concentrations during weekends due to reduced NO_x emissions, which limits O_3 titration). However, in JAS, this effect is slightly degraded with CAMS-REG-TEMPO, despite NO_2 correlation improvements during the same season. This illustrates the complexity of the O_3 cycle, which exhibits non-linear relationships with its main precursors, NO_x and VOCs. Similar to the monthly cycle, the diurnal cycle correlation coefficient remains largely unchanged across all seasons (Fig. 14). The ENS and all the individual models consistently show strong performance in reproducing the observed O_3 diurnal cycle, especially during AMJ and JAS (ENS correlation: 0.95), when concentrations are at their maximum. The low sensitivity of O_3 modelled cycle concentrations to changes in the emission temporal profiles can also be partially explained by the importance of O_3 hemispheric contributions to European background levels (Garatachea et al., 2024).

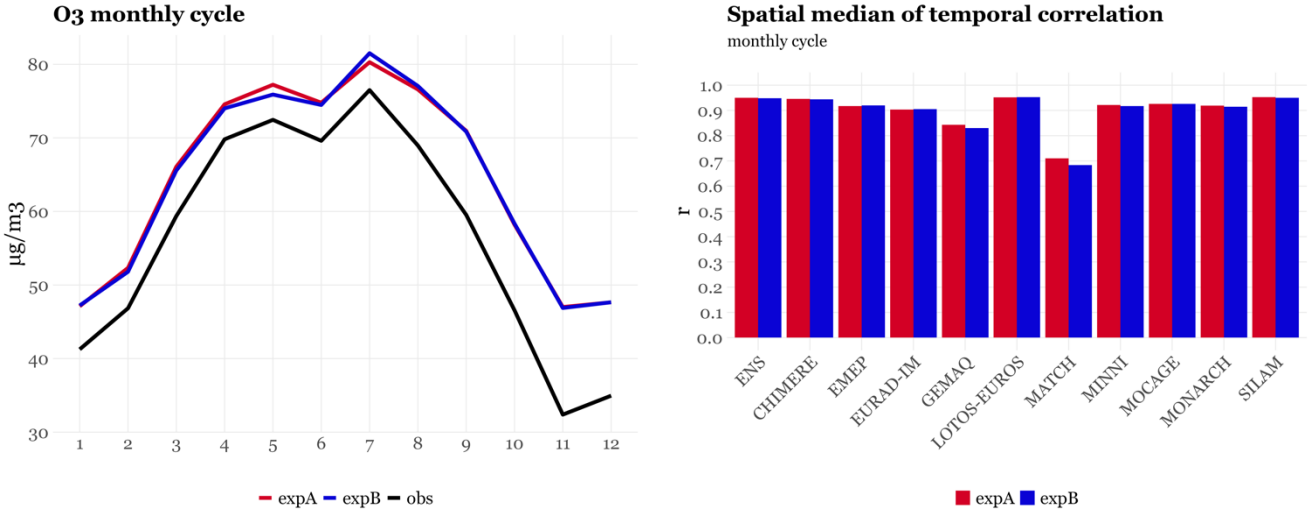

Figure 12 Comparison between the observed and modelled O_3 monthly cycle for the ENS (left) and spatial median of the temporal correlations obtained for the ENS and each individual CAMS model in expA (red) and expB (blue).

https://doi.org/10.5194/egusphere-2025-1287
Preprint. Discussion started: 11 April 2025

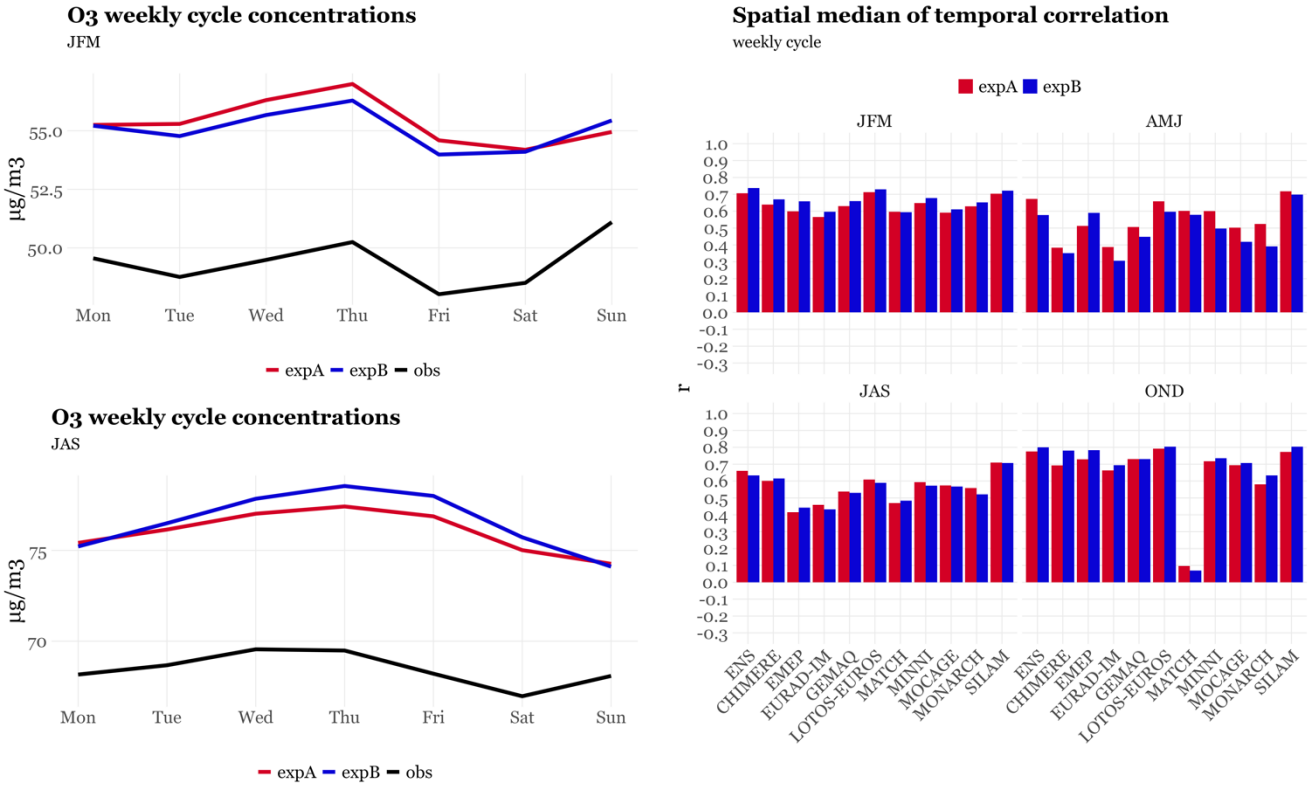

Figure 13 Comparison between the observed and modelled O_3 weekly cycle for the ENS for JFM and JAS (left) and spatial median of the temporal correlations obtained for the ENS and each individual CAMS model per season in expA (red) and expB (blue).

https://doi.org/10.5194/egusphere-2025-1287
Preprint. Discussion started: 11 April 2025

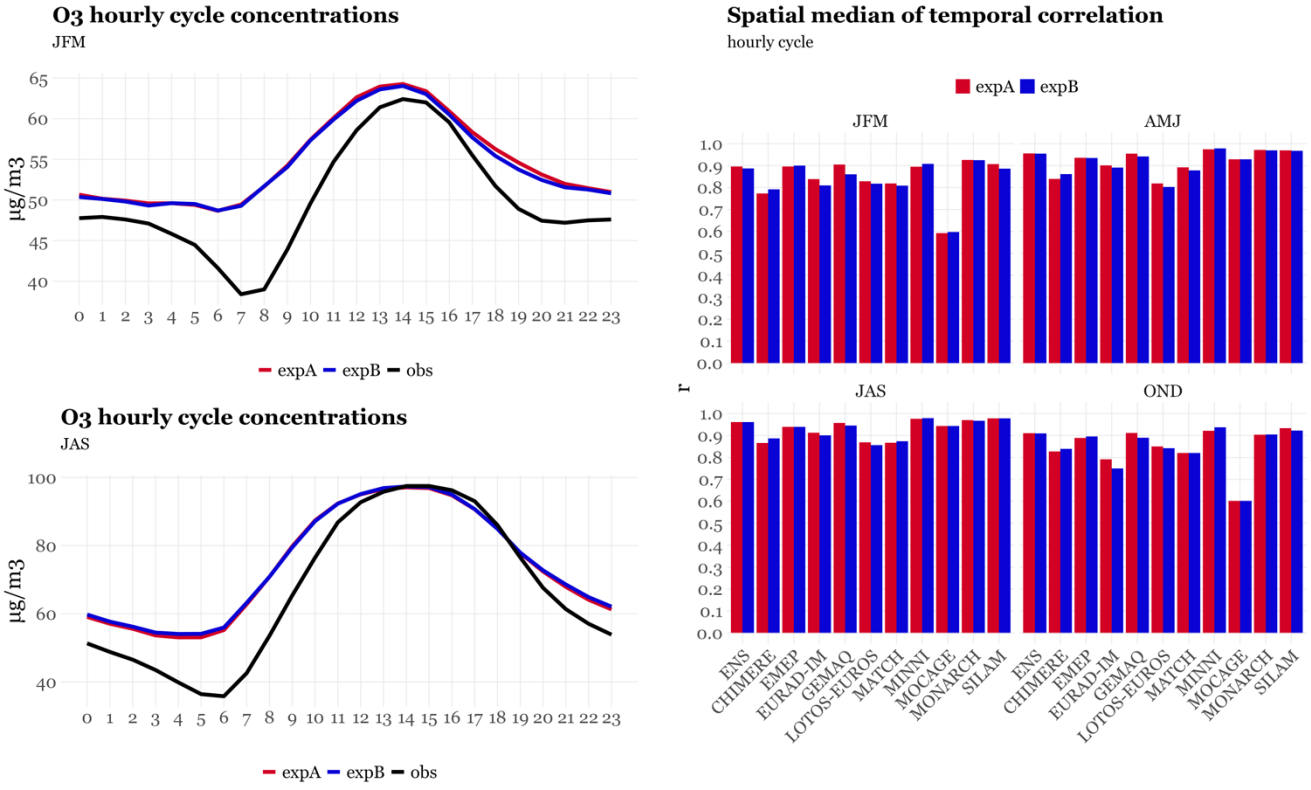

Figure 14 Comparison between the observed and modelled O_3 diurnal cycle for the ENS (UTC time) for JFM and JAS (left) and spatial median of the temporal correlations obtained for the ENS and each individual CAMS model per season in expA (red) and expB (blue).

3.2.3 PM_{10}

The correlation coefficient of the PM_{10} monthly cycle shows a slight improvement in the ENS and most individual models (8 out of 11), with an increase up to 0.09 in MATCH (fig. 15). The unrealistic peak modelled in April by expA, which is not observed in measurements, is significantly smoothed when using CAMS-REG-TEMPO profiles. This improvement is linked to a reduction of more than 20% in primary PM_{10} emissions in April under CAMS-REG-TEMPO, compared to the default profiles. A slight degradation is observed in models using the GENEMIS profiles in expA, for which correlation decrease by -0.07 (CHIMERE) and -0.03 (EMEP).

For weekly profiles, a consistent slight improvement is observed for ENS and across individual CAMS models during JFM and OND, when PM_{10} concentrations are at their maximum (Fig. 16). The largest improvements are reported during JFM by EMEP (+0.07) and MINNI (+0.05). Additionally, the bias between models and observations is slightly reduced in OND, as CAMS-REG-TEMPO allocates more PM_{10} emissions in November and December compared to the default profiles (Fig. S1).

https://doi.org/10.5194/egusphere-2025-1287
Preprint. Discussion started: 11 April 2025

Similar to NO_2, the impact of CAMS-REG-TEMPO on the PM_{10} diurnal cycle is heterogeneous across seasons (Fig. 17). A significant improvement is observed during OND, with the correlation coefficient increasing by over 50% for GEM-AQ and DEHM, and by more than 25% for LOTOS-EUROS, CHIMERE and MINNI. The improvement is less pronounced during JFM, with correlation increases of up to 10%. During JFM and OND, CAMS-REG-TEMPO better reproduces the observed evening peak, which is typically higher than the morning peak, especially in OND. In contrast, TNO and GENEMIS profiles tend of overestimate the morning peak relative to the evening peak. The enhanced performance of CAMS-REG-TEMPO can be mainly attributed to its diurnal profiles for residential and commercial combustion emissions, which concentrate emissions in the evening, whereas TNO and GENEMIS distribute emissions more evenly between morning and afternoon peaks (Fig. 6). However, the use of CAMS-REG-TEMPO diurnal profiles also increases the negative bias in the modelled morning PM_{10} peak. We partly attribute this bias to the omission of road transport resuspension emissions in the CAMS-REG-ANT inventory, as these are currently excluded in official reporting despite being reported as a significant contributor to the PM_{10} primary emissions in Europe (e.g., Denier van der Gon et al., 2018).

A shift of approximately two hours between the modelled and measured PM_{10} morning peak is observed both in the expA and expB ENS results. Further investigations should be performed to understand the causes behind this discrepancy, which could be partially associated with limitations in the models in reproduction the PBL and the formation of secondary aerosols.

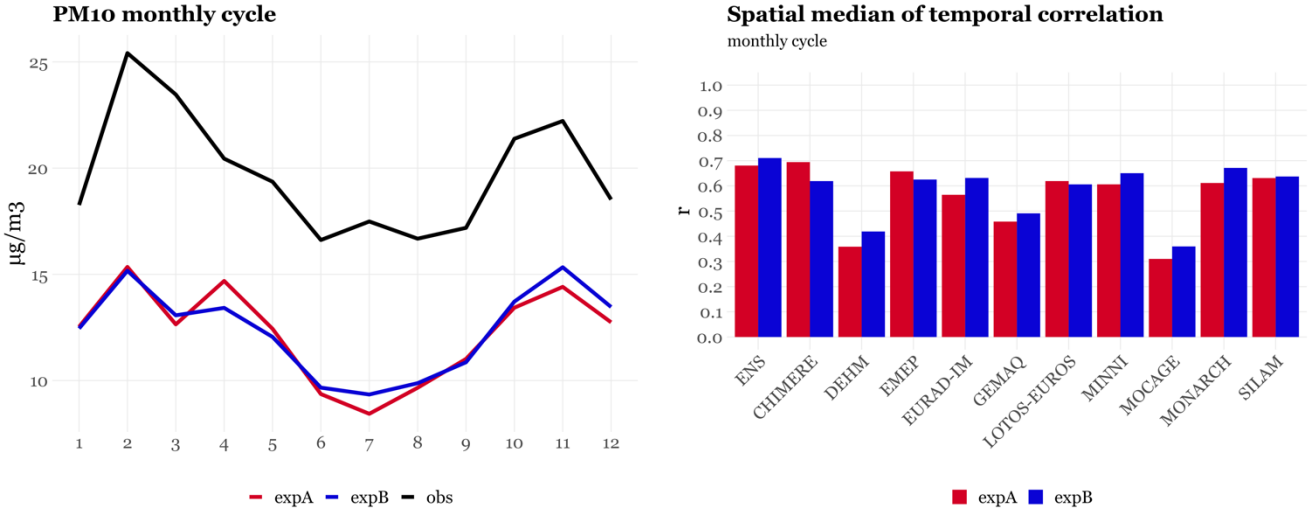

Figure 15 Comparison between the observed and modelled PM_{10} monthly cycle for the ENS (left) and spatial median of the temporal correlations obtained for the ENS and each individual CAMS model in expA (red) and expB (blue).

https://doi.org/10.5194/egusphere-2025-1287
Preprint. Discussion started: 11 April 2025

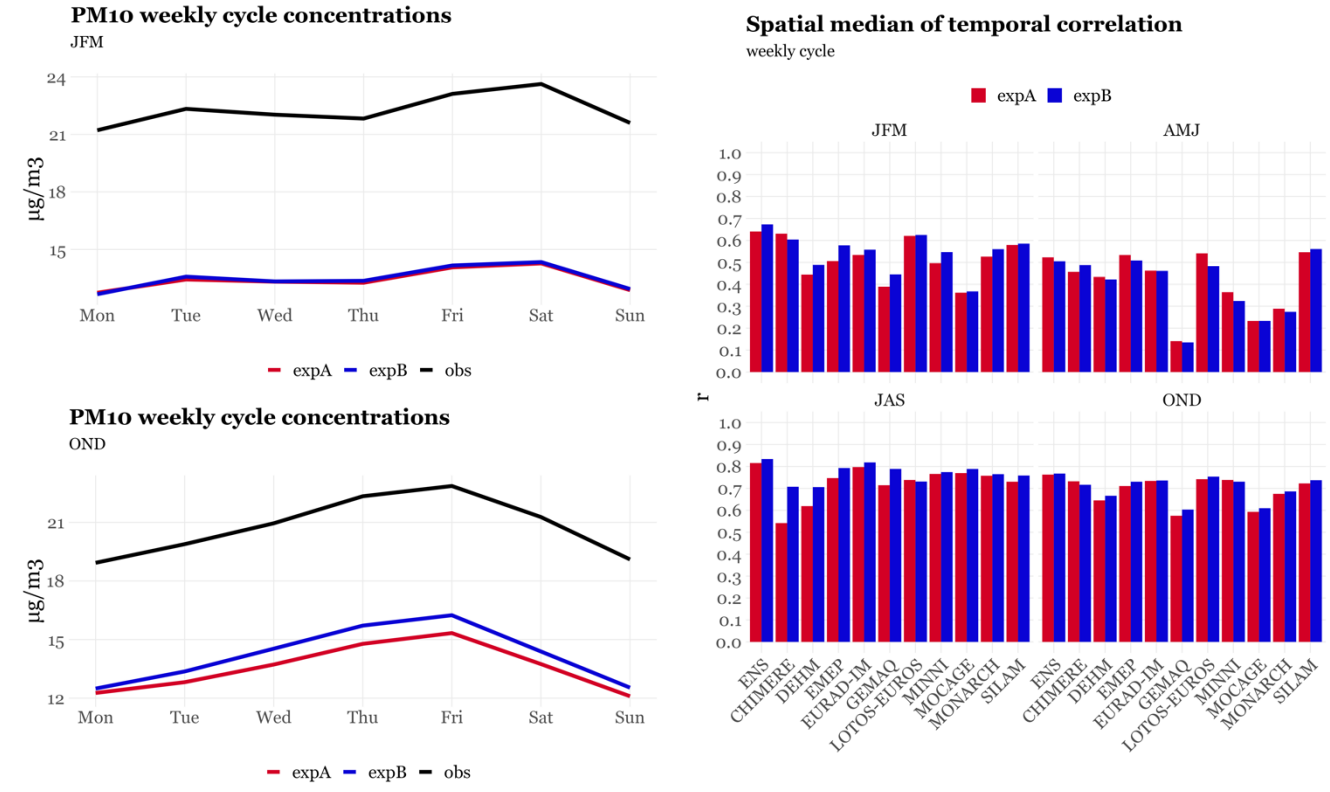

Figure 16 Comparison between the observed and modelled PM_{10} weekly cycle for the ENS for JFM and OND (left) and spatial median of the temporal correlations obtained for the ENS and each individual CAMS model per season in expA (red) and expB (blue).

https://doi.org/10.5194/egusphere-2025-1287
Preprint. Discussion started: 11 April 2025

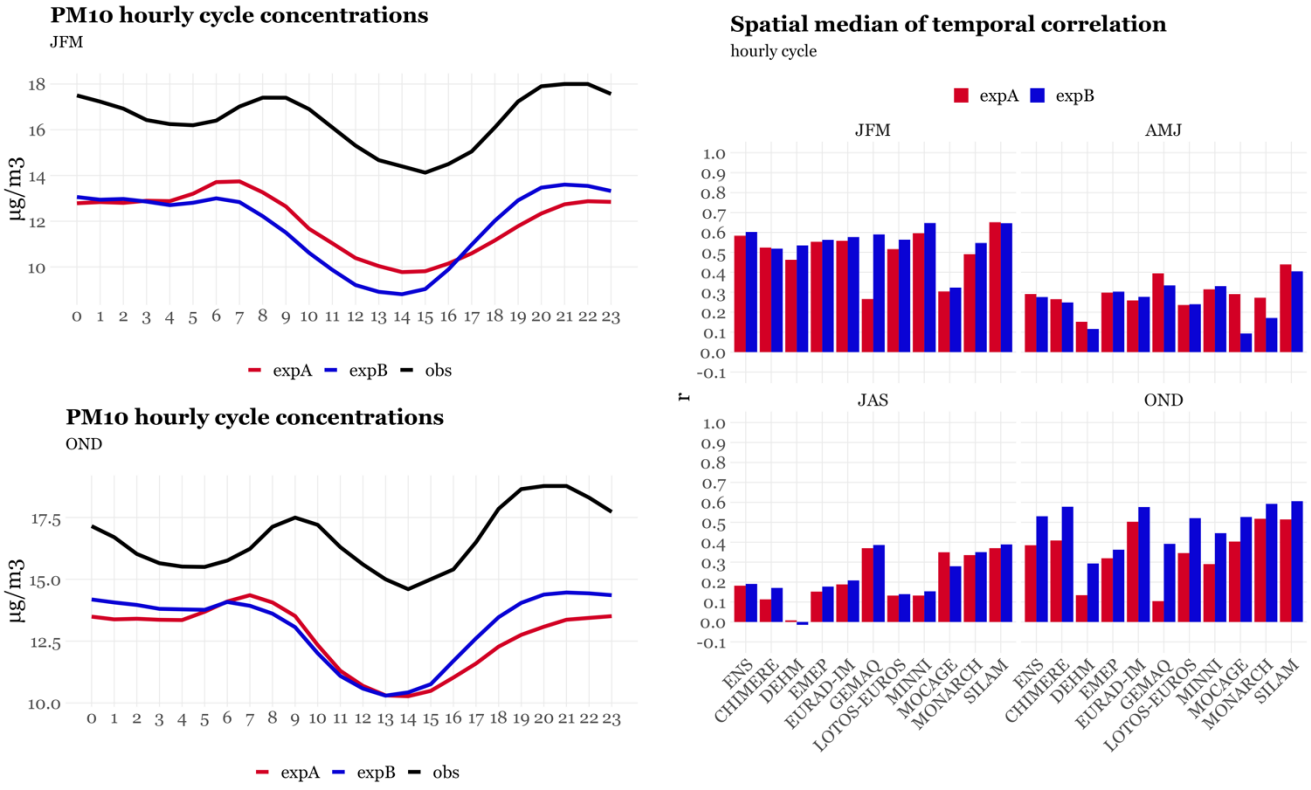

555 **Figure 17 Comparison between the observed and modelled PM_{10} diurnal cycle (UTC time) for the ENS for JFM and OND (left) and spatial median of the temporal correlations obtained for the ENS and each individual CAMS model per season in expA (red) and expB (blue).**

https://doi.org/10.5194/egusphere-2025-1287
Preprint. Discussion started: 11 April 2025

3.2.4 $PM_{2.5}$

For $PM_{2.5}$ there is no significant variation in the correlation coefficient for the monthly cycle in the ENS (+0.01) (Fig. 18). The CAMS models using the TNO profiles by default tend to present significant improvements (up to +0.10 and +0.08 EURAD-IM and for MOCAGE, respectively) while a degradation is observed in those models using GENEMIS by default, with correlation decreases up to -0.10 in the case of CHIMERE and -0.04 in the case of EMEP. It is important to note that the EEA observational coverage for $PM_{2.5}$ is less comprehensive in some countries (e.g., Spain, Italy) compared to other pollutants analysed (Fig. 8), which may influence these results.

For the weekly cycle (Fig. 19), the ENS shows an average correlation decrease of -0.04 in AMJ with expB and a slight increase of +0.02 in OND. During the other two seasons, the weekly cycle correlation remains unchanged for the ENS, reflecting a balance between improvements and degradations across individual models (e.g., +0.06 for DEHM vs. -0.08 for CHIMERE in JFM).

At the hourly scale (Fig. 20), results closely resemble those observed for PM_{10}. While there is a slight correlation decrease in AMJ (-0.01 on average for the ENS), a considerable increase is observed in OND (+0.15 on average for the ENS). As mentioned above, this improvement is mainly driven by the diurnal profile for residential combustion emissions in CAMS-REG-TEMPO. The two hours shift between modelled and measured morning peaks is also noticeable here, as reported for PM_{10}.

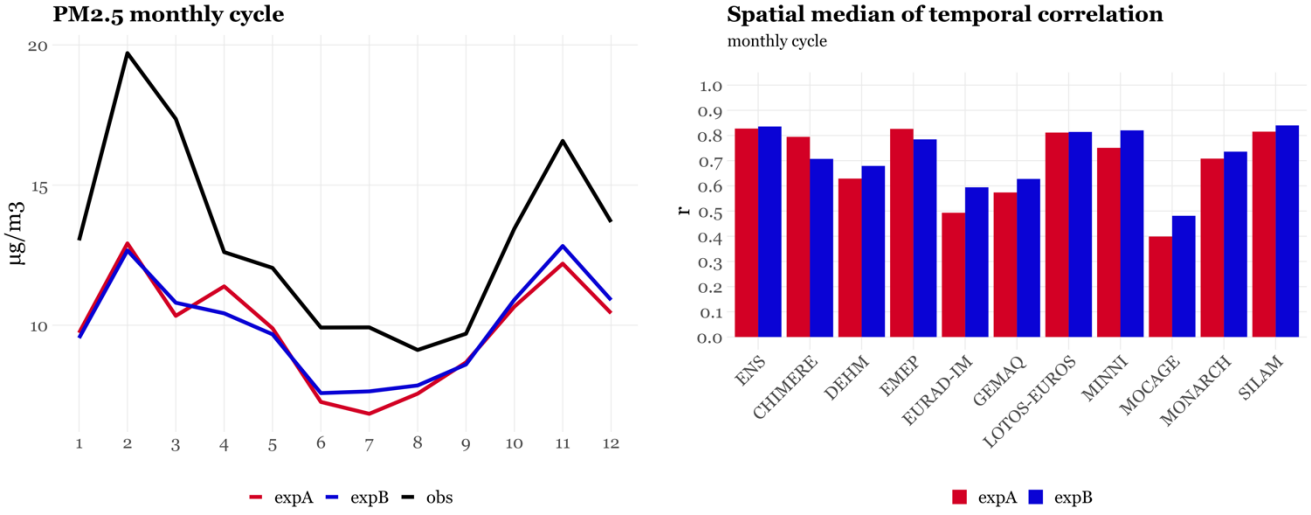

Figure 18 Comparison between the observed and modelled $PM_{2.5}$ monthly cycle for the ENS (left) and spatial median of the temporal correlations obtained for the ENS and each individual CAMS model in expA (red) and expB (blue).

https://doi.org/10.5194/egusphere-2025-1287
Preprint. Discussion started: 11 April 2025

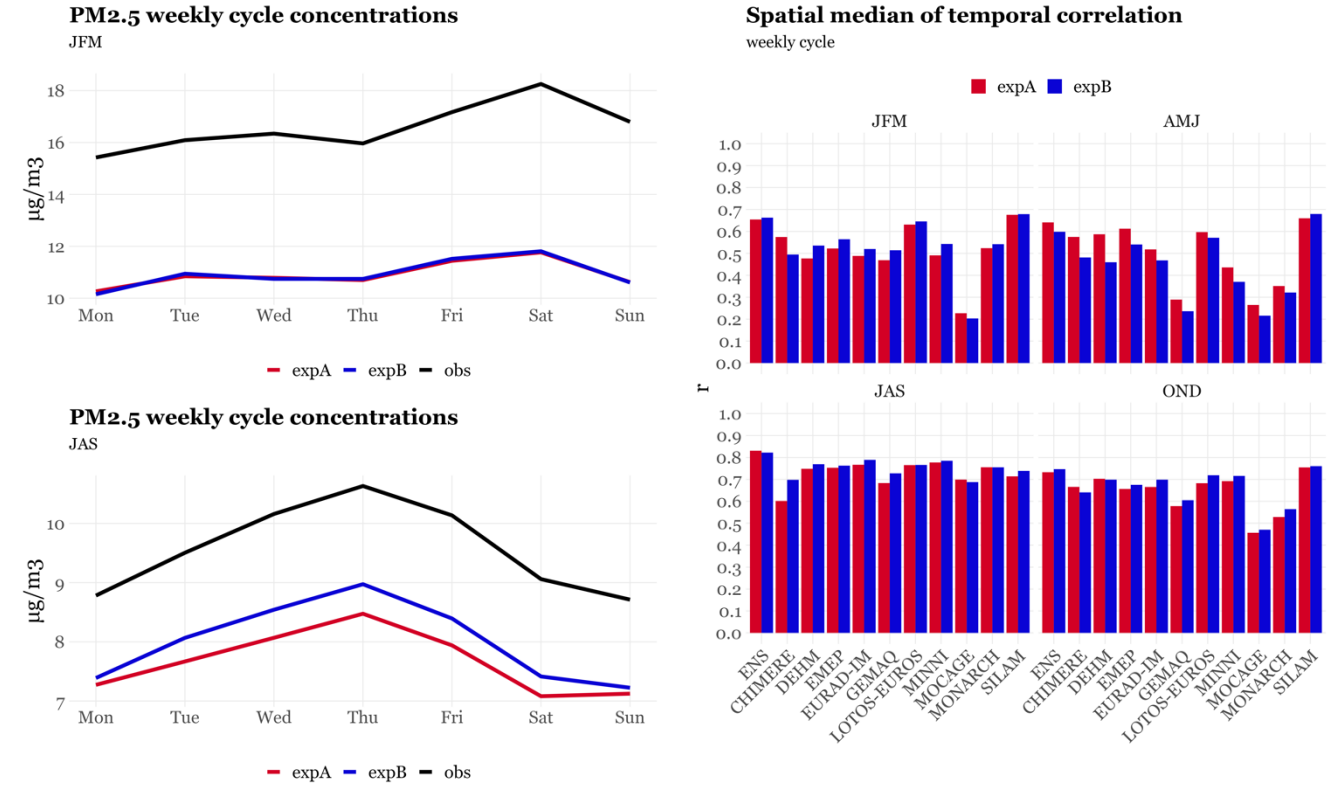

Figure 19 Comparison between the observed and modelled $PM_{2.5}$ weekly cycle for the ENS for JFM and JAS (left) and spatial median of the temporal correlations obtained for the ENS and each individual CAMS model per season in expA (red) and expB (blue).

https://doi.org/10.5194/egusphere-2025-1287
Preprint. Discussion started: 11 April 2025

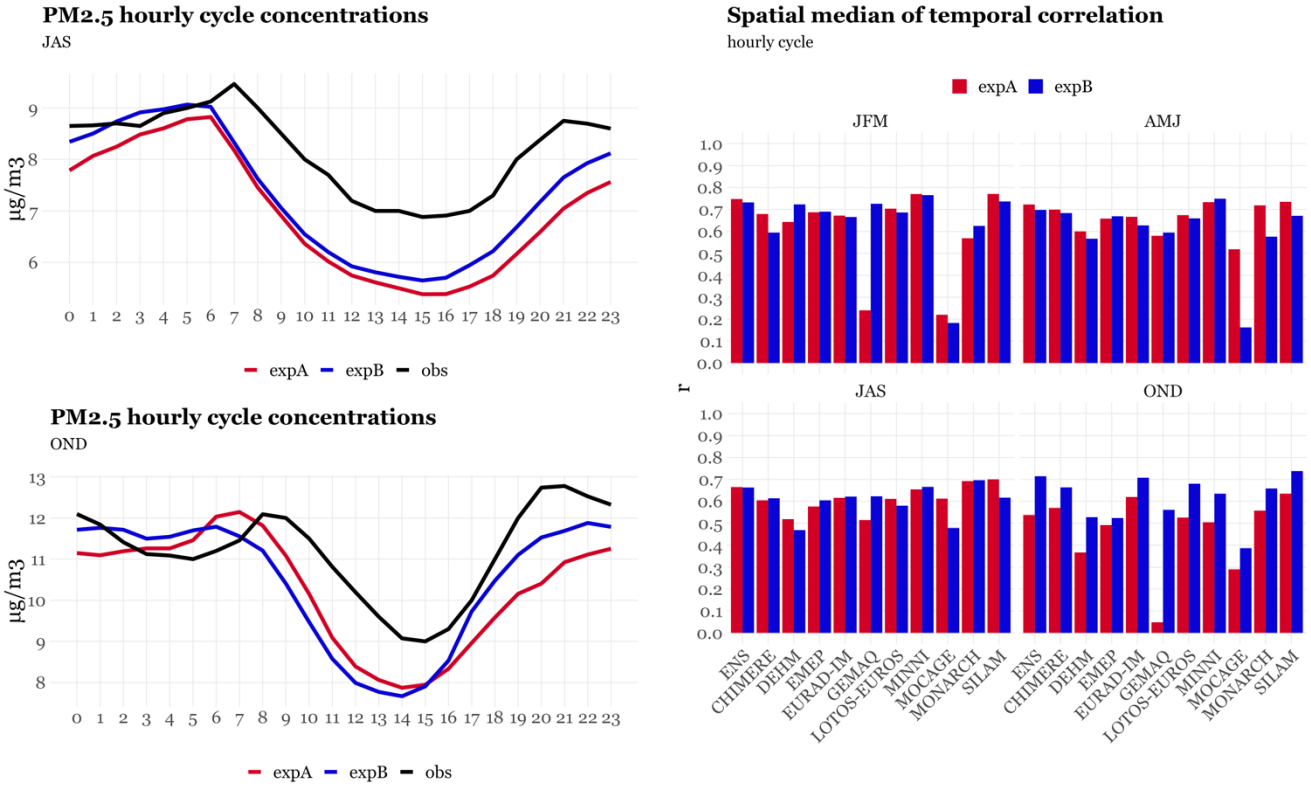

Figure 20 Comparison between the observed and modelled $PM_{2.5}$ diurnal cycle for the ENS (UTC time) for JAS and OND (left) and spatial median of the temporal correlations obtained for the ENS and each individual CAMS model per season in expA (red) and expB (blue).

https://doi.org/10.5194/egusphere-2025-1287
Preprint. Discussion started: 11 April 2025

3.3 Average deviation from observations

Figure 21 shows the annual spatial median of bias and RMSE computed by concentration intervals for the ENS across species for expA and expB. Overall, the statistics hardly vary between experiments, although slight decreases in both bias and RMSE are observed at higher concentration ranges, especially for PM_{10}, when comparing expB to expA.

Unlike annual averages, concentrations can vary significantly between seasons. For O_3, which exhibits a high seasonal variation, significant differences emerge between expA and expB in certain seasons (Fig. 22). In AMJ, the median of the daily maximum concentration is lower with expB compared to expA (increasing the bias). Conversely, during summer, expB reports higher values, reducing the bias when compared to observations.

For PM2.5, modelled daily mean concentrations in expB are slightly lower than in expA during JMF, except for certain pollution episodes (i.e., 8th February and 6th March). In contrast, concentrations are higher in JAS. This behaviour can be linked to the increase in primary PM2.5 emissions in summer under CAMS-REG-TEMPO compared to TNO or GENEMIS profiles. b Additionally, the rise in key precursors of secondary fine aerosols, such as NH_3 (Fig. 3 and 4), may also contribute to these differences.

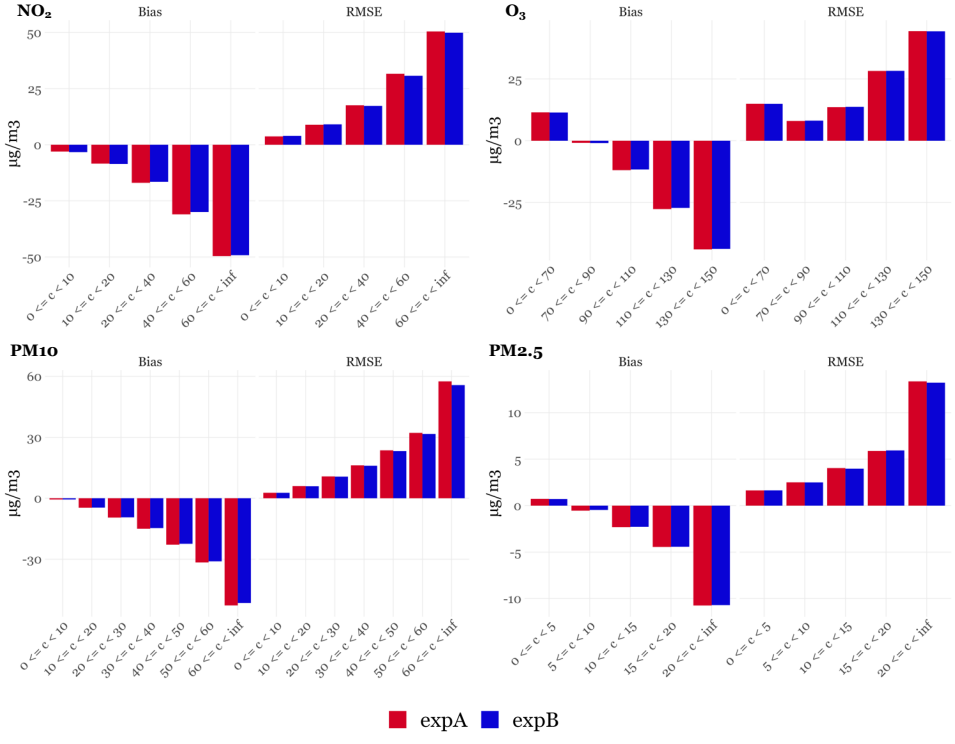

Figure 21 Spatial median of bias and RMSE computed by concentration intervals for the ENS per species (NO_2, O_3, PM10 and PM2.5) in expA (red) and expB (blue).

https://doi.org/10.5194/egusphere-2025-1287
Preprint. Discussion started: 11 April 2025

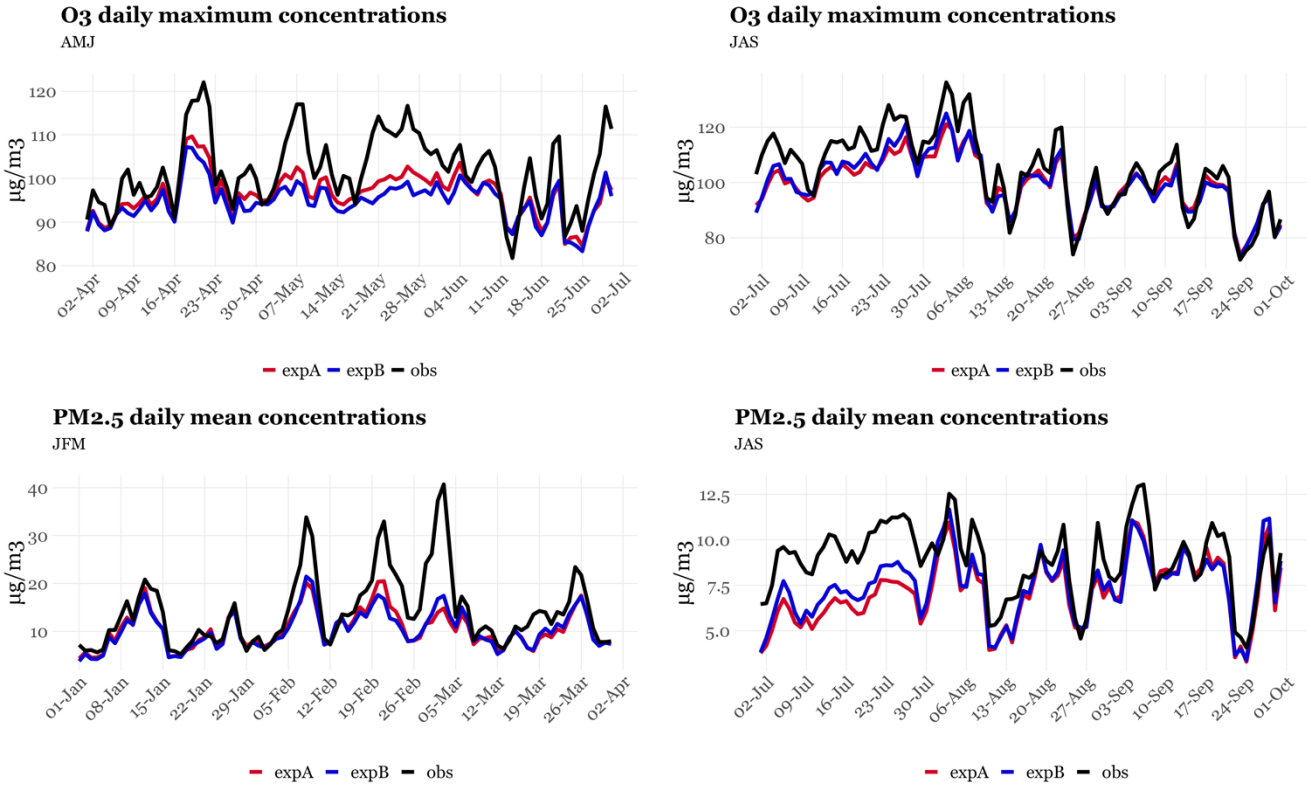

Figure 22 Spatial median of the observed (grey) and modelled (red, expA; blue expB) daily maximum concentration of O_3 by ENS during AMJ and JAS 2018 and daily mean concentration of PM2.5 during JFM and JAS 2018.

610

https://doi.org/10.5194/egusphere-2025-1287
Preprint. Discussion started: 11 April 2025

4 Conclusions

This study evaluates the impact of implementing updated anthropogenic emission temporal profiles on the performance scores of the CAMS European multi-model ensemble air quality modelling system. The CAMS-REG-TEMPO emission temporal profiles dataset was compared against the default temporal distributions considered in the 11 regional models that conform the CAMS ensemble, namely the TNO and GENEMIS profiles. The sensitivity of these models plus the ensemble (ENS, median of the 11 models) was assessed by comparing the simulation results with NO_2, O_3, $PM_{2.5}$ and PM_{10} observations from the EEA European air quality monitoring network. Model-observation comparisons were conducted for average hourly, weekly and monthly pollutant concentrations, analysed per season (JFM; AMJ, JAS, OND) to quantify the impact of CAMS-REG-TEMPO. The findings show that the effects of integrating CAMS-REG-TEMPO profiles vary depending on the pollutant and time cycle considered:

- NO_2 presents the greatest improvement in temporal correlation with CAMS-REG-TEMPO. The weekly cycle correlations present increases of up to +1.04 for one model and +0.06 (OND) to +0.16 (JFM) in the ENS. This improvement is mainly linked to the CAMS-REG-TEMPO weekly profiles for road transport. At the monthly scale, a better representation of the February NO_2 peak is observed due to the use of meteorological-dependent profiles. For the diurnal cycle, results vary considerably by model and the season. A positive impact is observed for the ENS (up to +0.07) and most models (up to +0.24) during JFM and OND, when NO_2 peaks. However, AMJ shows slight degradations, with correlation decreases of up to -0.18 in one model and -0.03 in the ENS.
- O_3 is least affected by changes in emission temporal profiles. Monthly and diurnal cycles remain almost unchanged across seasons, as O_3 correlation in the ENS are already high (between 0.9 and 0.95), leaving little the room for improvement. At weekly level, small correlation improvements are observed in JFM and OND (+0.03 for the ENS), while degradations occur in AMJ (-0.10) and JAS (-0.03). This contrast with NO_2 highlights the complexity of O_3 formation, its non-linear relationship with NO_x and VOCs and the importance of O_3 long range transport.
- PM_{10} is the only pollutant showing a notable improvement in the monthly cycle correlation (+0.03 in the ENS). Weekly cycle correlation improves slightly across the ENS and individual models in JFM and OND (up to +0.07), when PM10 concentrations peak. Diurnal cycle results are more heterogeneous, with significant improvements in OND (+0.13 for the ENS) and moderate improvement in JFM (+0.02 in the ENS). These improvements are mainly linked to the revised diurnal profile residential and commercial combustion emissions, which better capture the observed evening peak, typically larger than the morning peak.
- $PM_{2.5}$ results are more variable, depending on the model's default profiles. Models using the TNO profiles by default show significant improvements, whereas those using GEMINIS profiles show degradations, leading to an offset effect in the ENS. For weekly cycles, the ENS correlation remains unaltered in JFM and JAS, as improvements in some

https://doi.org/10.5194/egusphere-2025-1287
Preprint. Discussion started: 11 April 2025

models balance degradations in others. For the diurnal cycle, results resemble those of PM_{10}, with a considerable increase incorrelation during OND (+0.15 in the ENS).

- Annual RMSE and bias scores for ENS remain largely unaffected by CAMS-REG-TEMPO for all four pollutants, although slight decreases are observed at higher concentration ranges, especially for PM_{10}. While some seasonal differences emerge, these are minor compared to overall deviations from observations.
- The default temporal profiles differ across the 11 individual models, which partially explains the heterogeneous results observed. However, even among models using the same default profiles, contrasting responses to CAMS-REG-TEMPO are sometimes observed. For instance, NO_2 diurnal cycle correlations show opposite trends across models, which illustrates the complex interactions between temporal emission distributions and other physical and chemical processes such as the planetary boundary layer depth cycle. These findings align with previous air quality modelling intercomparisons exercises, where model spread persisted despite the use of common input parameters (e.g., Bessagnet et al., 2016).
- Overall, results indicate that the less the pollutant is directly linked to primary emissions, the lower is its sensitivity to changes in the emission temporal profiles. Improvements are particularly important for NO_2, and to a lesser extent PM_{10}, which are dominated by primary sources, while $PM_{2.5}$ and O_3 present a lower sensitivity due to a higher role of secondary formation and, in the case of O_3, of the remote influences due to its higher lifetime.

All in all, the use of the CAMS-REG-TEMPO emission temporal profiles offers performance results encouraging enough to support their implementation in the operational CAMS multi-model ensemble production. As a matter of fact, several teams have already implemented them in their models (e.g., Ge et al., 2024; Menu et al., 2024; Soussé-Villa et al., 2024). Some of the profiles reported in the CAMS-REG-TEMPO dataset are based on meteorological parametrisations, such as the Heating Degree Days, which can significantly change between years. As discussed in detail in Guion et al., (2024), the implementation of online versions of these parametrisations within the CAMS models is recommended to improve the performance of models when used in forecasting mode. Future works will focus on evaluating the impact of CAMS-REG-TEMPO on other modelled species, including pollutants of emerging concern such as black carbon, NH_3 and individual NMVOC species, which may provide additional insights and allow identifying opportunities for improvement and further refinement of the proxies and parametrisations currently considered to compute the profiles. We also plan to explore the development of new profiles for those activities for which we are still relying on data from the late nineties and that present significant contributions to primary emissions, namely NMVOC emissions from the use of solvent sector. Improvements will focus on investigating the inclusion of temperature-dependencies, as reported by recent studies such as Wu et al. (2024).

https://doi.org/10.5194/egusphere-2025-1287
Preprint. Discussion started: 11 April 2025

5 Code availability

The Python package evaltools used to perform the evaluation of the modelling results can be downloaded from the following site: https://opensource.umr-cnrm.fr/projects/evaltools (last accessed: March 2025).

6 Data availability

The CAMS-REG-AP_v4.2 gridded emission maps are accessible via https://doi.org/10.24380/0vzb-a387 (last accessed: March 2025). The CAMS-REG-TEMPO_v3.2 temporal profiles are available at https://doi.org/10.5281/zenodo.15011343 (last accessed: March 2025) (Guevara et al., 2025). Data on measurement stations from EEA can be downloaded at https://eeadmz1-downloads-webapp.azurewebsites.net/ (last accessed: March 2025).

7 Author contribution

MG designed and drafted the overall manuscript, prepared the figures and coordinated all contributions. AC coordinated the air quality modelling intercomparison exercise. VP performed the evaluation of the air quality modelling results against observations. All co-authors contributed to the production of the air quality modelling results and to the discussion of the results.

8 Competing interests

The authors declare that they have no conflict of interest.

9 Acknowledgements

The research leading to these results has received funding from the Copernicus Atmosphere Monitoring Service (CAMS), which is implemented by the European Centre for Medium-Range Weather Forecasts (ECMWF) on behalf of the European Commission. AU acknowledges support of EU Horizon project CAMAERA (grant 101134927). BSC acknowledges support from the Department of Research and Universities of the Government of Catalonia via the Research Group Atmospheric Composition (code 2021 1090 SGR 01550). YP acknowledges the contribution of the EU Horizon project CATALYSE (grant 101057131). MS acknowledges the RCF project VFSP-WASE (grant 359421). FZJ ICE-3 gratefully acknowledges computing time on the supercomputer JURECA (Jülich Supercomputing Centre, 2021) at Forschungszentrum Jülich under grant no. cjicg21. The computing resources and the related technical support for MINNI are provided by CRESCO/ENEAGRID High Performance Computing infrastructure and its staff. CRESCO/ENEAGRID High Performance Computing infrastructure is

https://doi.org/10.5194/egusphere-2025-1287
Preprint. Discussion started: 11 April 2025

funded by ENEA, the Italian National Agency for New Technologies, Energy and Sustainable Economic Development and by Italian and European research programmes (see http://www.cresco.enea.it/english).

https://doi.org/10.5194/egusphere-2025-1287
Preprint. Discussion started: 11 April 2025

10 References

Andersson, C., Langner, J., & Bergstroumm, R. (2007). Interannual variation and trends in air pollution over Europe due to climate variability during 1958–2001 simulated with a regional CTM coupled to the ERA40 reanalysis. Tellus B: Chemical and Physical Meteorology, 59(1), 77-98. https://onlinelibrary.wiley.com/doi/epdf/10.1111/j.1600-0889.2006.00196.x#:~:text=DOI%3A-,10.1111/j.1600%2D0889.2006.00196.x,-for%20NO

Athanasopoulou, E., Speyer, O., Brunner, D., Vogel, H., Vogel, B., Mihalopoulos, N., and Gerasopoulos, E.: Changes in domestic heating fuel use in Greece: effects on atmospheric chemistry and radiation, Atmos. Chem. Phys., 17, 10597–10618, https://doi.org/10.5194/acp-17-10597-2017, 2017.

Backes, A., Aulinger, A., Bieser, J., Matthias, V., and Quante, M.: Ammonia emissions in Europe, part I: Development of a dynamical ammonia emission inventory, Atmos. Environ., 131, 55–66, https://doi.org/10.1016/j.atmosenv.2016.01.041, 2016.

Badia, A., Jorba, O., Voulgarakis, A., Dabdub, D., Pérez García-Pando, C., Hilboll, A., Gonçalves, M., and Janjic, Z.: Description and evaluation of the Multiscale Online Nonhydrostatic AtmospheRe CHemistry model (NMMB-MONARCH) version 1.0: gas-phase chemistry at global scale, Geoscientific Model Development, 10, 609-638, 2017.

Baek, B. H., Coats, C., Ma, S., Wang, C.-T., Li, Y., Xing, J., Tong, D., Kim, S., and Woo, J.-H.: Dynamic Meteorology-induced Emissions Coupler (MetEmis) development in the Community Multiscale Air Quality (CMAQ): CMAQ-MetEmis, Geosci. Model Dev., 16, 4659–4676, https://doi.org/10.5194/gmd-16-4659-2023, 2023.

Bessagnet, B., Pirovano, G., Mircea, M., Cuvelier, C., Aulinger, A., Calori, G., Ciarelli, G., Manders, A., Stern, R., Tsyro, S., García Vivanco, M., Thunis, P., Pay, M.-T., Colette, A., Couvidat, F., Meleux, F., Rouïl, L., Ung, A., Aksoyoglu, S., Baldasano, J. M., Bieser, J., Briganti, G., Cappelletti, A., D'Isidoro, M., Finardi, S., Kranenburg, R., Silibello, C., Carnevale, C., Aas, W., Dupont, J.-C., Fagerli, H., Gonzalez, L., Menut, L., Prévôt, A. S. H., Roberts, P., and White, L.: Presentation of the EURODELTA III intercomparison exercise – evaluation of the chemistry transport models' performance on criteria pollutants and joint analysis with meteorology, Atmos. Chem. Phys., 16, 12667–12701, https://doi.org/10.5194/acp-16-12667-2016, 2016.

Brandt, J., Silver, J.D., Frohn, L.M., Geels, C., Gross, A., Hansen, A.B., Hansen, K.M., Hedegaard, G.B., Skjøth, C.A., Villadsen, H., Zare, A. and Christensen, J.H., 2012: "An integrated model study for Europe and North America using the Danish Eulerian Hemispheric Model with focus on intercontinental transport of air pollution". Atmospheric Environment, Vol. 53, pp. 156-176.

Christensen, J.H., 1997: "The Danish Eulerian Hemispheric Model - a Three-Dimensional Air Pollution Model Used for the Arctic". Atmospheric Environment, Vol. 31, No. 24, pp. 4169-4191.

Colette, A., Collin, G., Besson, F., Blot, E., Guidard, V., Meleux, F., Royer, A., Petiot, V., Miller, C., Fermond, O., Jeant, A., Adani, M., Arteta, J., Benedictow, A., Bergström, R., Bowdalo, D., Brandt, J., Briganti, G., Carvalho, A. C., Christensen, J. H., Couvidat, F., D'Elia, I., D'Isidoro, M., Denier van der Gon, H., Descombes, G., Di Tomaso, E., Douros, J., Escribano, J., Eskes, H., Fagerli, H., Fatahi, Y., Flemming, J., Friese, E., Frohn, L., Gauss, M., Geels, C., Guarnieri, G., Guevara, M., Guion,

A., Guth, J., Hänninen, R., Hansen, K., Im, U., Janssen, R., Jeoffrion, M., Joly, M., Jones, L., Jorba, O., Kadantsev, E., Kahnert, M., Kaminski, J. W., Kouznetsov, R., Kranenburg, R., Kuenen, J., Lange, A. C., Langner, J., Lannuque, V., Macchia, F., Manders, A., Mircea, M., Nyiri, A., Olid, M., Pérez García-Pando, C., Palamarchuk, Y., Piersanti, A., Raux, B., Razinger, M., Robertson, L., Segers, A., Schaap, M., Siljamo, P., Simpson, D., Sofiev, M., Stangel, A., Struzewska, J., Tena, C., Timmermans, R., Tsikerdekis, T., Tsyro, S., Tyuryakov, S., Ung, A., Uppstu, A., Valdebenito, A., van Velthoven, P., Vitali, L., Ye, Z., Peuch, V.-H., and Rouïl, L.: Copernicus Atmosphere Monitoring Service – Regional Air Quality Production System v1.0, EGUsphere [preprint], https://doi.org/10.5194/egusphere-2024-3744, 2024.

Copernicus Climate Change Service (C3S): State-of-the-European-climate: February 2018, available at: https://surfobs.climate.copernicus.eu/stateoftheclimate/february2018.php, (last access: July 2024) 2018.

Crippa, M., Guizzardi, D., Muntean, M., Schaaf, E., Dentener, F., van Aardenne, J. A., Monni, S., Doering, U., Olivier, J. G. J., Pagliari, V., and Janssens-Maenhout, G.: Gridded emissions of air pollutants for the period 1970–2012 within EDGAR v4.3.2, Earth Syst. Sci. Data, 10, 1987–2013, doi:10.5194/essd-10-1987-2018, 2018.

D'Elia, I., Briganti, G., Vitali, L., Piersanti, A., Righini, G., D'Isidoro, M., Cappelletti, A., Mircea, M., Adani, M., Zanini, G., and Ciancarella, L.: Measured and modelled air quality trends in Italy over the period 2003–2010, Atmos. Chem. Phys., 21, 10825–10849, https://doi.org/10.5194/acp-21-10825-2021, 2021.

Denier van der Gon, H. A. C., Hendriks, C., Kuenen, J., Segers, A., and Visschedijk, A. J. H.: Description of current temporal emission patterns and sensitivity of predicted AQ for temporal emission patterns, EU FP7 MACC deliverable report D_D-EMIS_1.3, available at: https://atmosphere.copernicus.eu/sites/default/files/2019-07/MACC_TNO_del_1_3_v2.pdf (last access: February 2021), 2011.

Denier van der Gon, H., Hulskotte, J., Jozwicka, M., Kranenburg, R., Kuenen, J. and Visschedijk, A.: Chapter 5 - European emission inventories and projections for road transport non-exhaust emissions: Analysis of consistency and gaps in emission inventories from EU member states. F. Amato (Ed.), Non-Exhaust Emissions, Academic Press (2018), pp. 101-121, 10.1016/B978-0-12-811770-5.00005-4.

Ding, J., van der A, R., Eskes, H., Dammers, E., Shephard, M., Wichink Kruit, R., Guevara, M., and Tarrason, L.: Ammonia emission estimates using CrIS satellite observations over Europe, Atmos. Chem. Phys., 24, 10583–10599, https://doi.org/10.5194/acp-24-10583-2024, 2024.

Ebel, A., Friedrich, R., and Rodhe, H.: GENEMIS: Assessment, Improvement, and Temporal and Spatial Disaggregation of European Emission Data, in Tropospheric Modelling and Emission Estimation: Chemical Transport and Emission Modelling on Regional, Global and Urban Scales, edited by: Ebel, A., Friedrich, R., and Rodhe, H., Springer Berlin Heidelberg, Berlin, Heidelberg, 181–214, https://doi.org/10.1007/978-3-662-03470-5_6, 1997.

EMEP/CEIP: Present state of emission data, available at: https://www.ceip.at/webdab-emission-database/reported-emissiondata (last access: July 2024), 2021.

EMEP/EEA: Air pollutant emission inventory guidebook 2019, Technical guidance to prepare national emission inventories, EEA Report No 13/2019, available at: https://www.eea.europa.eu/publications/emep-eea-guidebook-2019 (last access: July 2024), 2019.

EMEP MSC-W: Open Source EMEP/MSC-W model rv4.45 (202203), doi:10.5281/zenodo.8337953, 2022.

EUROCONTROL: European Organisation for the Safety of Air Navigation. Operations at airports, https://ansperformance.eu/data/, last access: July 2024, 2020.

Fatahi, Y., Kouznetsov, R., and Sofiev, M.: The effect of accounting for public holidays on the skills of the atmospheric composition model SILAM v.5.7, Geosci. Model Dev., 14, 7459–7475, https://doi.org/10.5194/gmd-14-7459-2021, 2021.

Flemming, J., Huijnen, V., Arteta, J., Bechtold, P., Beljaars, A., Blechschmidt, A.-M., Diamantakis, M., Engelen, R. J., Gaudel, A., Inness, A., Jones, L., Josse, B., Katragkou, E., Marecal, V., Peuch, V.-H., Richter, A., Schultz, M. G., Stein, O., and Tsikerdekis, A.: Tropospheric chemistry in the Integrated Forecasting System of ECMWF, Geosci. Model Dev., 8, 975–1003, https://doi.org/10.5194/gmd-8-975-2015, 2015.

Franke, P, Lange, A.C., Steffens, B, Pozzer, A, Wahner, A, Kiendler-Scharr, A.: European air quality in view of the WHO 2021 guideline levels: Effect of emission reductions on air pollution exposure. Elementa: Science of the Anthropocene 12(1). DOI: https://doi.org/10.1525/elementa.2023.00127, 2024.

Friedrich, R. and Reis, S.: Emissions of Air Pollutants – Measurements, Calculation, Uncertainties – Results from the EUROTRAC-2 Subproject GENEMIS, Springer Publishers, Berlin, Heidelberg, Germany, 2004.

Friese, E. and Ebel, A.: Temperature Dependent Thermodynamic Model of the System H+ - NH4+ - Na+ - SO42- - NO3- Cl- - H2O, J. Phys. Chem. A, 114, 11595-11631, DOI:10.1021/JP101041J, 2010.

Frohn, L.M., Christensen, J.H. and Brandt, J., 2002: "Development of a High-Resolution Nested Air Pollution Model: The Numerical Approach", Journal of Computational Physics, Vol. 179, pp. 68-94.

Frohn, L.M., Ketzel, M., Christensen, J.H., Brandt, J., Im, U., Massling, A., Andersen, C., Plejdrup, M.S., Nielsen, O.-K., van der Gon, H.D., Manders, A. and Raaschou-Nielsen, O., 2021: "Modelling ultrafine particle number concentrations at address resolution in Denmark from 1979-2018 – Part 1: Regional and urban scale modelling and evaluation". Atmospheric Environment, Vol. 264, 118631, https://doi.org/10.1016/j.atmosenv.2021.118631

Galmarini, S., Kioutsioukis, I., and Solazzo, E.: E pluribus unum*: ensemble air quality predictions, Atmos. Chem. Phys. 13, pp. 7153-7182, doi:10.5194/acp-13-7153-2013, 2013.

Garatachea, R., Pay, M.T., Achebak, H., Jorba, O., Bowdalo, D., Guevara, M., Petetin, H., Ballester, J., and Pérez García-Pando, C.: National and transboundary contributions to surface ozone concentration across European countries. Commun Earth Environ 5, 588, https://doi.org/10.1038/s43247-024-01716-w, 2024.

Ge, Y., Solberg, S., Heal, M. R., Reimann, S., van Caspel, W., Hellack, B., Salameh, T., and Simpson, D.: Evaluation of modelled versus observed non-methane volatile organic compounds at European Monitoring and Evaluation Programme sites in Europe, Atmos. Chem. Phys., 24, 7699–7729, https://doi.org/10.5194/acp-24-7699-2024, 2024.

https://doi.org/10.5194/egusphere-2025-1287
Preprint. Discussion started: 11 April 2025

Geels, C., Winther, M., Andersson, C., Jalkanen, J.-P., Brandt, J., Frohn, L.M., Im, U., Leung, W. and Christensen, J.H.: Projections of shipping emissions and the related impact on air pollution and human health in the Nordic region. Atmospheric Chemistry and Physics, Vol. 21, 12495-12519, https://doi.org/10.5194/acp-21-12495-2021, 2021.

Grythe, H., Lopez-Aparicio, S., Vogt, M., Vo Thanh, D., Hak, C., Halse, A. K., Hamer, P., and Sousa Santos, G.: The MetVed model: development and evaluation of emissions from residential wood combustion at high spatio-temporal resolution in Norway, Atmos. Chem. Phys., 19, 10217–10237, https://doi.org/10.5194/acp-19-10217-2019, 2019.

Guevara, M., Tena, C., Porquet, M., Jorba, O., and Pérez García-Pando, C.: HERMESv3, a stand-alone multi-scale atmospheric emission modelling framework – Part 1: global and regional module, Geosci. Model Dev., 12, 1885–1907, https://doi.org/10.5194/gmd-12-1885-2019, 2019.

Guevara, M., Jorba, O., Tena, C., Denier van der Gon, H., Kuenen, J., Elguindi, N., Darras, S., Granier, C., and Pérez García-Pando, C.: Copernicus Atmosphere Monitoring Service TEMPOral profiles (CAMS-TEMPO): global and European emission temporal profile maps for atmospheric chemistry modelling, Earth Syst. Sci. Data, 13, 367–404, https://doi.org/10.5194/essd-13-367-2021, 2021.

Guevara, M., Jorba, O., & Pérez García-Pando, C. (2025). CAMS-REG-TEMPOv3.2 (v3.2) [Data set]. Zenodo. https://doi.org/10.5281/zenodo.15011343

Guion, A., Couvidat, F., Guevara, M., and Colette, A.: Country and species-dependent parameters for the Heating Degree Day method to distribute NOx and PM emissions from residential heating in the EU-27: application to air quality modelling and multi-year emission projections, EGUsphere [preprint], https://doi.org/10.5194/egusphere-2024-2911, 2024.

Guth, J., Josse, B., Marécal, V., Joly, M., and Hamer, P.: First implementation of secondary inorganic aerosols in the MOCAGE version R2.15.0 chemistry transport model, Geosci. Model Dev., 9, 137–160, https://doi.org/10.5194/gmd-9-137-2016, 2016.

Jalkanen, J.-P., Johansson, L., and Kukkonen, J.: A comprehensive inventory of ship traffic exhaust emissions in the European sea areas in 2011, Atmos. Chem. Phys., 16, 71–84, https://doi.org/10.5194/acp-16-71-2016, 2016.

Joly, M. and Peuch, V.-H.: Objective classification of air quality monitoring sites over Europe, Atmos. Environ., 47, 111–123, https://doi.org/10.1016/j.atmosenv.2011.11.025, 2012.

Josse, B., Simon, P. and Peuch, V.-H.: Radon global simulations with the multiscale chemistry and transport model MOCAGE, Tellus B: Chemical and Physical Meteorology, 56(4), 339–356. https://doi.org/10.3402/tellusb.v56i4.16448, 2004.

Jülich Supercomputing Centre: JURECA: Data Centric and Booster Modules implementing the Modular Supercomputing Architecture at Jülich Supercomputing Centre Journal of large-scale research facilities, 7, A182. http://dx.doi.org/10.17815/jlsrf-7-182, 2021.

Kaiser, J. W., Heil, A., Andreae, M. O., Benedetti, A., Chubarova, N., Jones, L., Morcrette, J.-J., Razinger, M., Schultz, M. G., Suttie, M., and van der Werf, G. R.: Biomass burning emissions estimated with a global fire assimilation system based on observed fire radiative power, Biogeosciences, 9, 527–554, https://doi.org/10.5194/bg-9-527-2012, 2012.

https://doi.org/10.5194/egusphere-2025-1287
Preprint. Discussion started: 11 April 2025

Kaminski, J.W., L. Neary, J. Struzewska, J.C. McConnell, A. Lupu, J. Jarosz, K. Toyota, S.L. Gong, J. Côté, X. Liu, K. Chance, and A. Richter: GEM-AQ, an on-line global multiscale chemical weather modelling system: model description and evaluation of gas phase chemistry processes. Atmos. Chem. Phys., 8, 3255-3281, 2008.

Klose, M., Jorba, O., Gonçalves Ageitos, M., Escribano, J., Dawson, M. L., Obiso, V., Di Tomaso, E., Basart, S., Montané Pinto, G., and Macchia, F.: Mineral dust cycle in the Multiscale Online Nonhydrostatic AtmospheRe CHemistry model (MONARCH) version 2.0, Geoscientific Model Development, 14, 6403-6444, 2021.

Kouznetsov, R., Sofiev, M., 2012. A methodology for evaluation of vertical dispersion and dry deposition of atmospheric aerosols. Journal of Geophysical Research 117. https://doi.org/doi:10.1029/2011JD016366

Lenhart, L., Friedrich, R. European emission data with high temporal and spatial resolution. Water Air Soil Pollut 85, 1897–1902. https://doi.org/10.1007/BF01186111, 1995.

Manders, A. M. M., Builtjes, P. J. H., Curier, L., Denier van der Gon, H. A. C., Hendriks, C., Jonkers, S., Kranenburg, R., Kuenen, J. J. P., Segers, A. J., Timmermans, R. M. A., Visschedijk, A. J. H., Wichink Kruit, R. J., van Pul, W. A. J., Sauter, F. J., van der Swaluw, E., Swart, D. P. J., Douros, J., Eskes, H., van Meijgaard, E., van Ulft, B., van Velthoven, P., Banzhaf, S., Mues, A. C., Stern, R., Fu, G., Lu, S., Heemink, A., van Velzen, N., and Schaap, M.: Curriculum vitae of the LOTOS–EUROS (v2.0) chemistry transport model, Geosci. Model Dev., 10, 4145–4173, https://doi.org/10.5194/gmd-10-4145-2017, 2017.

de Meij, A., Cuvelier, C., Thunis, P., and Pisoni, E.: A new set of indicators for model evaluation complementing to FAIRMODE's MQO, EGUsphere [preprint], https://doi.org/10.5194/egusphere-2024-3690, 2025.

Menut, L., Goussebaile, A., Bessagnet, B., Khvorostiyanov, D., and Ung, A.: Impact of realistic hourly emissions profiles on air pollutants concentrations modelled with CHIMERE, Atmos. Environ., 49, 233–244, https://doi.org/10.1016/j.atmosenv.2011.11.057, 2012.

Menut, L., Bessagnet, B., Briant, R., Cholakian, A., Couvidat, F., Mailler, S., Pennel, R., Siour, G., Tuccella, P., Turquety, S., and Valari, M.: The CHIMERE v2020r1 online chemistry-transport model, Geosci. Model Dev., 14, 6781–6811, https://doi.org/10.5194/gmd-14-6781-2021, 2021.

Menut, L., Cholakian, A., Pennel, R., Siour, G., Mailler, S., Valari, M., Lugon, L., and Meurdesoif, Y.: The CHIMERE chemistry-transport model v2023r1, Geosci. Model Dev., 17, 5431–5457, https://doi.org/10.5194/gmd-17-5431-2024, 2024.

Mircea, M., Ciancarella, L., Briganti, G., Calori, G., Cappelletti, A., Cionni, I., Costa, M., Cremona, G., D'Isidoro, M., Finardi, S., Pace, G., Piersanti, A., Righini, G., Silibello, C., Vitali, L., and Zanini, G.: Assessment of the AMS-MINNI system capabilities to simulate air quality over Italy for the calendar year 2005, Atmospheric Environment, 84, 178-188, https://doi.org/10.1016/j.atmosenv.2013.11.006, 2014.

Mues, A., Kuenen, J., Hendriks, C., Manders, A., Segers, A., Scholz, Y., Hueglin, C., Builtjes, P., and Schaap, M.: Sensitivity of air pollution simulations with LOTOS-EUROS to the temporal distribution of anthropogenic emissions, Atmos. Chem. Phys., 14, 939–955, https://doi.org/10.5194/acp-14-939-2014, 2014.

Navarro-Barboza, H., Pandolfi, M., Guevara, M., Enciso, S., Tena, C., Via, M., Yus-Díez, J., Reche, C., Pérez, N., Alastuey, A., Querol, X., and Jorba, O.: Uncertainties in source allocation of carbonaceous aerosols in a Mediterranean region, Environment International, 183, 108 252, https://doi.org/10.1016/j.envint.2023.108252, 2024.

Pérez, C., Haustein, K., Janjic, Z., Jorba, O., Huneeus, N., Baldasano, J. M., Black, T., Basart, S., Nickovic, S., Miller, R. L., Perlwitz, J. P., Schulz, M., and Thomson, M.: Atmospheric dust modeling from meso to global scales with the online NMMB/BSC-Dust model – Part 1: Model description, annual simulations and evaluation, Atmos. Chem. Phys., 11, 13001–13027, https://doi.org/10.5194/acp-11-13001-2011, 2011.

Pesaresi, M., Florczyk, A., Schiavina, M., Melchiorri, M., Maffenini, L.: GHS-SMOD R2019A - GHS settlement layers, updated and refined REGIO model 2014 in application to GHS-BUILT R2018A and GHS-POP R2019A, multitemporal (1975-1990-2000-2015). European Commission, Joint Research Centre (JRC) [Dataset] doi: 10.2905/42E8BE89-54FF-464E-BE7B-BF9E64DA5218 PID: http://data.europa.eu/89h/42e8be89-54ff-464e-be7b-bf9e64da5218, 2019.

Sič, B., El Amraoui, L., Marécal, V., Josse, B., Arteta, J., Guth, J., Joly, M., and Hamer, P. D.: Modelling of primary aerosols in the chemical transport model MOCAGE: development and evaluation of aerosol physical parameterizations, Geosci. Model Dev., 8, 381–408, https://doi.org/10.5194/gmd-8-381-2015, 2015.

Skjøth, C. A., Geels, C., Berge, H., Gyldenkærne, S., Fagerli, H., Ellermann, T., Frohn, L. M., Christensen, J., Hansen, K. M., Hansen, K., and Hertel, O.: Spatial and temporal variations in ammonia emissions – a freely accessible model code for Europe, Atmos. Chem. Phys., 11, 5221–5236, https://doi.org/10.5194/acp-11-5221-2011, 2011.

Sofiev, M., 2002. Extended resistance analogy for construction of the vertical diffusion scheme for dispersion models. JGR-Atmospheres, 107, ACH 10-1-ACH 10-8. https://doi.org/10.1029/2001JD001233

Soussé-Villa, R., Jorba, O., Gonçalves Ageitos, M., Bowdalo, D., Guevara, M., and Pérez García-Pando, C.: A Comprehensive Global Modelling Assessment of Nitrate Heterogeneous Formation on Desert Dust, EGUsphere [preprint], https://doi.org/10.5194/egusphere-2024-2310, 2024.

Robertson, L., J. Langner, and M. Engardt, 1999: An Eulerian Limited-Area Atmospheric Transport Model. J. Appl. Meteor. Climatol., 38, 190–210, https://doi.org/10.1175/1520-0450(1999)038<0190:AELAAT>2.0.CO;2

Sofiev, M., Genikhovich, E., Keronen, P., Vesala, T., 2010. Diagnosing the Surface Layer Parameters for Dispersion Models within the Meteorological-to-Dispersion Modeling Interface. Journal of Applied Meteorology and Climatology 49, 221–233. https://doi.org/10.1175/2009JAMC2210.1

Simpson, D., Benedictow, A., Berge, H., Bergström, R., Emberson, L. D., Fagerli, H., Hayman, G. D., Gauss, M., Jonson, J. E., Jenkin, M. E., Nyíri, A., Richter, C., Semeena, V. S., Tsyro, S., Tuovinen, J.-P., Valdebenito, A., and Wind, P.: The EMEP MSC-W chemical transport model – technical description, Atmos. Chem. Physics, 12, 7825–7865, doi:10.5194/acp-12-7825-2012, 2012.

Sofiev, M., Vira, J., Kouznetsov, R., Prank, M., Soares, J., Genikhovich, E., 2015. Construction of an Eulerian atmospheric dispersion model based on the advection algorithm of M. Galperin: dynamic cores v.4 and 5 of SILAM v.5.5. Geoscientific Model Development 8, 3497–3522. https://doi.org/10.5194/gmd-8-3497-2015

https://doi.org/10.5194/egusphere-2025-1287
Preprint. Discussion started: 11 April 2025

Sofiev, M., Winebrake, J.J., Johansson, L., Carr, E.W., Prank, M., Soares, J., Vira, J., Kouznetsov, R., Jalkanen, J.-P., Corbett, J.J., 2018. Cleaner fuels for ships provide public health benefits with climate tradeoffs. Nat Commun 9, 406. https://doi.org/10.1038/s41467-017-02774-9

Struzewska, J. and J.W. Kaminski: Formation and transport of photooxidants over Europe during the July 2006 heat wave - observations and GEM-AQ model simulations, Atmos. Chem. Phys., 8, 721-736, 2008.

Super, I., Dellaert, S. N.C., Tokaya, J.P., and Schaap, M.: The impact of temporal variability in prior emissions on the optimization of urban anthropogenic emissions of CO2, CH4 and CO using in-situ observations, Atmospheric Environment: X, 11, https://doi.org/10.1016/j.aeaoa.2021.100119, 2021.

Veldt, C.: Updating and upgrading the PHOXA emission data base to 1990, TNO report, Netherlands Organisation for Applied Scientific Research, Apeldoorn, 92–118, 1992.

Wu, W., Fu, T.-M., Arnold, S.R., Spracklen, D.V., Zhang, A., Tao, W., Wang, X., Hou, Y., Mo, J., Chen, J., Li, Y., Feng, X., Lin, H., Huang, Z., Zheng, J., Shen, H., Zhu, L., Wang, C., Ye, J., and Yang, X.: Temperature-Dependent Evaporative Anthropogenic VOC Emissions Significantly Exacerbate Regional Ozone Pollution. Environmental Science & Technology 2024 58 (12), 5430-5441, doi: 10.1021/acs.est.3c09122, 2024.